TAMPEREEN TEKNILLINEN YLIOPISTO
TAMPERE UNIVERSITY OF TECHNOLOGY

MARKUS LAHIKAINEN

THE EFFECT OF GOLD NANOROD DOPING IN OPTICAL-TO-MECHANICAL ENERGY CONVERSION IN LIQUID-CRYSTAL ELASTOMERS

Master of Science Thesis

Examiners:
Prof. Arri Priimägi
D. Sc. (Tech.) Matti Virkki
Examiners and topic approved by the Faculty Council of the Faculty of Natural Sciences
on 9th November 2016

ABSTRACT

MARKUS LAHIKAINEN: The Effect of Gold Nanorod Doping in Optical-to-Mechanical Energy Conversion in Liquid-Crystal Elastomers
Tampere University of Technology
Master of Science Thesis, 62 pages, 2 Appendix pages
December 2016
Master's Degree Programme in Science and Engineering
Major: Chemistry
Examiners: Prof. Arri Priimägi and D. Sc. (Tech.) Matti Virkki

Keywords: gold nanorod, liquid-crystal elastomer, photo-mechanical actuator plasmonic, functionalization

Smart stimuli-responsive materials that can be externally triggered to undergo mechanical motions have a huge potential in applications ranging from artificial muscles and sensing to microrobotics. Among different classes of stimuli-responsive materials, photomechanical actuators based on liquid-crystal elastomers (LCEs) are of particular importance because they provide a route to control mechanical motions with light. Liquid-crystal elastomers exhibit a unique combination of anisotropic molecular order due to liquid crystallinity, and elasticity brought about by the polymer network. This coupling leads to the ability of free-standing LCE samples to change their shape reversibly after the application of external stimulus. Plasmonic nanoparticles, for example gold nanorods, have the ability to absorb light strongly at different wavelengths, depending on their dimensions, which makes them a possible candidate to produce the light response needed to actuate LCEs.

In the Thesis work three photoactuable liquid-crystal elastomers, which absorb light in different wavelengths, were studied. Infrared-absorbing gold nanorods, cross-linked UV-absorbing azobenzenes, and doped visible-absorbing azobenzenes, were used as light-absorbing moieties. The LCE that was used was acrylate-based and the sample films were prepared by applying well-developed liquid crystal-alignment technologies and photopolymerization.

As a major part of this work, gold nanorods were synthesized and functionalized. Gold nanorods were synthesized with a seed-mediated growth method in water by using hexadecylcetyltrimethylammonium bromide as a surfactant and 5-bromosalisylic acid as an additive. Rods were also synthesized without the additive for comparison and it was found that nanorods synthesized with the additive had smaller size dispersion and better morphology. Gold nanorods were successfully functionalized and transferred to organic solutions with dodecanethiol when thiolated polyethylene glycol was used for pre-functionalization. The solubility of the functionalized gold nanorods into LCE mixture (comprising photopolymerizable monomer and cross-linker) was studied. However, functionalized gold nanorods were not soluble into the LCE matrix, whereas the two dyes showed a good solubility and polymerized films could be efficiently actuated with light. The main characterization methods used in this work were UV-Vis-NIR spectroscopy, transmission electron microscopy, and polarized optical microscopy.

TIIVISTELMÄ

MARKUS LAHIKAINEN: Kultananosauvapohjaiset valomekaaniset nestekide-elastomeerit
Tampereen teknillinen yliopisto
Diplomityö, 62 sivua, 2 liitesivua
Joulukuu 2016
Teknis-luonnontieteellinen diplomi-insinöörin tutkinto-ohjelma
Pääaine: Kemia
Tarkastaja: Prof. Arri Priimägi ja TkT. Matti Virkki

Avainsanat: kultananosauva, nestekide-elastomeeri, valomekaniikka, funktionalisointi, plasmoniikka

Materiaaleilla, joita voidaan ulkoisesti stimuloida mekaaniseen liikkeeseen, on erittäin suuri sovelluspotentiaali muun muassa keinolihaksissa, antureissa ja robotiikassa. Etenkin valomekaaniset aktuaattorit, jotka perustuvat nestekide-elastomeereihin ovat erityisen mielenkiintoisia, sillä niiden avulla mekaaninen liike voidaan aikaansaada hyödyntämällä valoenergiaa. Nestekide-elastomeerit ovat materiaaleja, joiden molekyylit ovat järjestäytyneet nestekiteille tyypillisesti säännölliseksi rakenteeksi, mutta jotka ovat silti polymeeriverkostonsa ansiosta joustavia, kuten kumit. Tämän takia nestekide-elastomeerit voivat muuttaa muotoaan reversiibelisti ulkoisen ärsykkeen johdosta. Valoaktiivisen nestekide-elastomeerin valmistamiseen voidaan käyttää plasmonisia nanopartikkeleja, kuten kultananosauvoja. Kultananosauvat absorboivat valoa eri aallonpituuksilla, riippuen niiden mittasuhteesta, mikä tekee niistä erinomaisen vaihtoehdon nestekide-elastomeerien aktivoimiseen.

Tässä työssä tutkittiin kolmea erilaista valoaktiivista nestekide-elastomeeria, jotka absorboivat valoa eri aallonpituuksilla: infrapuna-aktiivisia kultananosauvoja, ultraviolettiaktiivisia asobentseeneja, jotka liitettiin polymeeriketjuun kovalentein sidoksin, sekä nestekide-elastomeerin sulautettuja, näkyvää valoa absorboivia asobentseeneja. Nestekide-elastomeerit olivat akrylaattipohjaisia, ja näytteiden valmistuksessa käytettiin nestekiteille tyypillistä valopolymerisointia nestekidemolekyylien yhtenäisen järjestyksen takaavassa kennossa.

Tämän työn laajin osuus keskittyi kultananosauvojen synteesiin ja funktionalisointiin. Kultananosauvat syntetisoitiin siemenkeskeisellä kasvatusmetodilla käyttämällä heksadekyylisetyylitrimetyyliammoniumbromidia pinta-aktiivisena aineena ja 5-bromosalisyylihappoa lisäaineena. Vertailun vuoksi sauvoja syntetisoitiin myös ilman lisäainetta, jolloin huomattiin, että sauvoilla, jotka syntetisoitiin lisäaineen kanssa, oli kapeampi kokojakauma ja parempi morfologia. Kultananosauvat funktionalisoitiin onnistuneesti dodekaanitiolilla, kun ensin suoritettiin esifunktionalisointi tioloidulla polyetyleeniglykolilla. Lisäksi tutkittiin funktionalisoitujen kultananosauvojen liukenemista nestekide-elastomeeri seoksen kanssa. Funktionalisoidut kultananosauvat eivät kuitenkaan liuenneet nestekide-elastomeerin, kun taas kaksi tutkittua väriainetta liukenivat hyvin ja polymerisoidut kalvot osoittivat valomekaanista vastetta. Tärkeimpinä tutkimusmetodeina työssä käytettiin UV-Vis-NIR spektroskopiaa, läpivalaisuelektronimikroskopiaa sekä polarisoitua optista mikroskopiaa.

PREFACE

This work has been carried out in the Chemistry Laboratory at the Department of Chemistry and Bioengineering at Tampere University of Technology in 2016. First of all, I would like to thank my supervisor Prof. Arri Priimägi for giving me the possibility to join the Smart Photonic Materials group and for providing me the opportunity to do this work. I am also grateful to him for giving me an unforgettable chance to visit a Summer School in France. I would also like to thank the co-supervisor Dr. Matti Virkki for his help on this Thesis. To Prof. Timo Laaksonen, I am thankful for his advice on gold nanorod synthesis and functionalization.

I am grateful to Mari Honkanen from the Materials Science Department at Tampere University of Technology. Her professional help with the transmission electron microscope has been invaluable and I thank her for taking the high-quality TEM pictures.

I would like to thank all the members of the Smart Photonic Materials group for supporting me and helping me with all the problems I faced during this work. In particular, I want the thank Dr. Hao Zeng and Mr. Owies Wani for their guidance and for being the best roommates.

For a pleasant work atmosphere, I am grateful to all colleagues of the Department of Chemistry and Bioengineering. I want to express my gratitude especially to Marja Asp-Lehtinen for her help and the long conversations that I had with her. Thanks also to Dr. Riikka Lahtinen for her help along the way, and to Anne Tikkanen for taking the care of practical matters.

To all my friends, who I have met at TUT over the years, I am also thankful for providing counterbalance to studies and this Thesis work. Finally, I would like to express my gratitude to my parents, grandmother, aunt, sisters and friends in Pieksämäki for the care and support along the way. They bring joy and balance to my life.

Tampere, 22.11.2016

Markus Lahikainen

CONTENTS

LIST OF SYMBOLS AND ABBREVIATIONS

AR	aspect ratio
CTAB	hexadecyltrimethylammonium bromide
DDT	dodecanethiol
DR1	Disperse Red 1
FWHM	full width at half maximum
GNR	gold nanorod
IR-LCE	liquid-crystal elastomer composition, which contains infrared-absorbing gold nanorods
LC	liquid crystal
LCE	liquid-crystal elastomer
LCN	liquid-crystal polymer network
mPEG-SH	poly(ethylene glycol) methyl ether thiol
N	nematic phase of liquid crystal
POM	polarized optical microscope
rpm	revolutions per minute
SmA	smectic A phase of liquid crystal
SmC	smectic C phase of liquid crystal
SPR	surface plasmon resonance
TEM	transmission electron microscopy
UV-LCE	liquid-crystal elastomer composition, which contains ultraviolet-absorbing cross-linking azobenzene
UV-Vis-NIR	ultraviolet-visible-near infrared
Vis-LCE	liquid-crystal elastomer composition, which contains visible light absorbing Disperse Red 1

A	absorbance
$A_{LSPR,max}$	maximum absorbance of the longitudinal surface plasmon resonance band
b	optical path of light
c	concentration
l	length of a gold nanorod
$\mathbf{n}$	local director of liquid crystal
S	order parameter
$T_{N/I}$	nematic-isotropic phase transition temperature
w	width of a gold nanorod
λ	wavelength
$\lambda_{LSPR,max}$	longitudinal surface plasmon resonance maximum wavelength
ε	molar absorption coefficient

1. INTRODUCTION

Photonics plays an important role in our everyday lives and drives innovation in an increasing number of fields such as telecommunications, medical technologies and home entertainment. Photonics can be found in the background of many familiar devices and technologies such as smartphones and the internet. Understanding the interaction between light and various types of materials is the key to the success of photonics. In recent years, **light-responsive liquid-crystal elastomers** as new photonics materials, have received increasing scientific attention [1]. The main thrust for this comes from their structural versatility and low cost, combined with the strong and fast response of organic molecules to optical fields.

Liquid crystal elastomers (LCEs) are loosely cross-linked polymer networks that combine rubber-like elasticity to the strong orientational anisotropy of liquid crystals (LCs) [2]. The most interesting property of LCEs is the ability to **change their shape reversibly** after the application of a certain external stimulus [3]. The external stimulus may be a change in temperature, electric or magnetic fields or electromagnetic radiation. LCE materials can work as an actuator, which is a system that converts energy from an input stimulus into mechanical motion. In this work, light is used to actuate LCE materials. Such actuators can produce clean, non-toxic and cheap optical-to-mechanical energy conversion, thereby enabling reversible actuation, without the requirement of physical contact between the energy source and the object. Potential applications of such LCE actuators include artificial muscles, micromechanics and microelectromechanical systems [3].

Most known light-responsive LCEs are designed to rely on reversible photoswitching of photochromic molecular units between two states, which have different structural and physical properties [4]. In order to translate effectively such molecular-level switching into macroscopic mechanical motions, the switching must take place in the solid state, and the switchable molecules must act in concert, which is provided by the liquid-crystal order. Such light-induced macroscopic phenomena are also known as photomechanical effects [4]. Nowadays most photomechanical actuators are based on *cis-trans* transformation of azobenzene dyes, which are actuated with ultraviolet light [1]. However, LCEs, which could be actuated with visible or infrared light, may have more applications as they would enable (i) the utilization of sunlight for actuation, and (ii) applications in biosciences. Yet they have been much less studied. One route for actuation with light in the visible or infrared wavelengths is to utilize photothermal effects. In a photothermal effect light is absorbed by an organic or inorganic dopant and then converted to heat, which

stimulates the shape changes of the LCE matrix. The dopant can be, *e.g.*, an organic molecule, a plasmonic nanoparticle, or a carbon-based nanomaterial such as carbon nanotube.

Gold nanoparticles are suitable for LCE actuation because of their unique shape-dependent localized surface plasmon resonance properties. Surface plasmons are the collective electron excitations induced by light at metallic-dielectric interfaces [5]. Due to the strong enhancement of the local electromagnetic fields close to the metal surface, surface plasmons can be used to manipulate light-matter interactions at the nanoscale [5]. In particular, gold nanorods (GNRs) are good candidates for photoactuation. GNRs are cylinder-shaped particles with length between 25 and 100 nm and width between 10 and 50 nm. Gold nanorods absorb light at different wavelengths depending on their dimensions and convert the absorbed light energy efficiently into thermal energy through photothermal effect. The produced thermal energy can heat the surrounding material effectively and provide the stimulation needed to activate the LCE.

In this Thesis, GNRs were synthesized and functionalized, and attempts were made to dope them into LCE networks aiming for photoactuated LCE materials. The purpose of the work was to compare actuation of the GNR-based LCE films with those containing azobenzene dyes, which have been more widely studied and can be actuated with UV or visible light, depending on the molecular structure. The first and the largest part of this work consists of the synthesis of the gold nanorods. The rods were synthesized using a **seed-mediated growth method** in which aqueous gold salt is reduced to metallic gold. The purpose was to synthesize rods that have main absorption peaks at around 800 nm and were coated with hexadecyltrimethylammonium bromide (CTAB). Because gold nanorods were synthesized with wet-chemical method, they were not soluble in organic LCE matrix. Therefore, re-functionalization had to be done. The second important part of this work was to study how GNRs dissolve with the acrylate-based liquid crystal molecules used in the photopolymerization method. LCE films doped with cross-linked UV-actuable azobenzenes and doped visible-absorbing azobenzenes were photopolymerized as well for comparison. Finally, actuation behavior of these materials was studied.

The overall structure of the Thesis takes the form of six chapters, which are divided between literature survey and experimental research. The literature survey in this Thesis has been divided into two main sections. Section 2 introduces the theoretical background of gold nanorods and Section 3 focuses on liquid-crystal elastomers as photoactuable materials. The experiments performed, together with their results and analysis, are discussed in Sections 4 and 5. Section 6 summarizes the main findings and outlines the key directions for future research stemming from this Thesis.

2. GOLD NANORODS

Gold nanorods are cylinder-shaped particles that have two axes: the transverse and the longitudinal axis [6]. Dimensions of the GNRs are between 10-150 nm and typically the length varies between 25 and 100 nm and the width between 10 and 50 nm [7; 8]. The ratio of the rods' length to width is called aspect ratio (AR) and it can be between 1 and 15 [9].

In this section, gold nanorods and their special optical properties are discussed, followed by a description of how rods can convert light into heat through photothermal effect. After that, the synthesis process and factors influencing the synthesis are described together with possibilities to tune the aspect ratio of the rods. Characterization and determination of the concentration of the GNR solutions are also discussed. Finally, surface functionalization of GNRs is described.

2.1 Optical properties of gold nanorods

Gold nanoparticles have been studied extensively because of their unique optical properties, which differ significantly from the corresponding properties of the bulk metals [5]. This difference results from the small size of the nanoparticles, significantly smaller than the wavelength of light (400-700 nm) [6]. The unique optical properties of gold nanoparticles render them ideal candidates for a wide range of applications in, *e.g.*, medicine, photonics, and biotechnology [10]. For example, significant work has been done in the direction of applying gold nanoparticles for sensing and detection of various analytics in biological and other systems [10].

Metal nanoparticles have the ability to **absorb and scatter light at different wavelengths with exceptional efficiency given their small size** [5]. Nanoparticles interact strongly with light, because conduction electrons of the nanoparticles oscillate with respect to their positive core due to the oscillating electric field of light. When the conduction electrons oscillate coherently, they displace an electron cloud from the nuclei, giving rise to a surface charge distribution as is shown in Figure 1 [6]. The Coulomb attraction between the electrons and the positive core results in a restoring force that causes the oscillation. At a certain frequency, the coherent oscillation is particularly strong. This resonant oscillation of the conduction electrons is called **surface plasmon resonance (SPR)**. The electrons oscillate between the two surfaces at the same frequency, which depends on the size, shape and local refractive index near the particle surface [5]. Because of the SPR, enormous local electromagnetic fields are produced around the nanoparticles and great enhancement of their radiative properties, such as absorption and scattering, can be achieved.

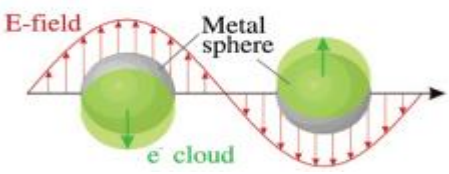

Figure 1. *Schematic picture of plasmon oscillation of a metal nanoparticle [6].*

Metal nanoparticles can absorb or scatter light. Total energy loss of light because of absorption and scattering is called extinction [11]. Mie-theory can be used to study the surface plasmon absorption, scattering and extinction of the metal nanoparticles [12]. According to Mie-theory, the size of the nanoparticles determines in which proportion they absorb and scatter light. Bigger nanoparticles tend to scatter more light than absorb it.

Gold nanorods are anisotropic particles which means that they have different dimensions in the transverse and longitudinal directions. This is why GNRs have two separate SPR modes corresponding to their width and length, known as the transverse and longitudinal surface plasmon resonances, respectively. Both of these SPR modes are presented in Figure 2a for a 45 nm long and 10 nm wide GNR. Both resonances occur in visible-infrared wavelengths (400-1200 nm). The transverse SPR is located close to 500 nm while the longitudinal resonance can vary widely between 600 and 1200 nm according to the GNR's aspect ratio and the overall size [10]. According to the Gans theory, optical properties of the GNRs are largely determined by their aspect ratio [5; 12]. In particular, there exists correlation between longitudinal SPR peak maximum wavelength and aspect ratio of the rods. As can been seen from Figure 2b this correlation is almost linear [8]. Because of this simple correlation, the **optical properties of GNRs can be tuned by simply varying the aspect ratio of the rods** [5; 9]. GNRs have a relatively large optical extinction coefficient ($\sim 1 \cdot 10^{-12} - 10 \cdot 10^{-12}$ cm^2 per rod) compared to their small size [6; 13]. Therefore, they absorb and scatter light efficiently and absorption peaks are clearly observed from the ultraviolet-visible-near infrared (UV-Vis-NIR) spectrum.

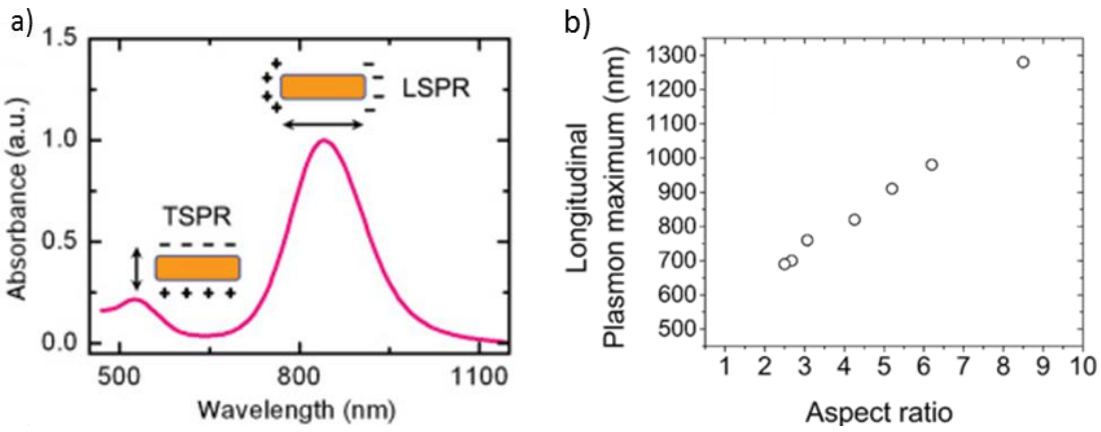

Figure 2. *a) UV-Vis-NIR absorption spectrum of GNR solution, which shows transverse surface plasmon resonance (TSPR) and longitudinal surface plasmon resonance (LSPR) modes corresponding to two absorption peaks [6]. b) Longitudinal plasmon maximum as a function of the GNR aspect ratio [8].*

The optical properties of GNRs also depend also on the refractive index near the particle surface [12; 14]. Because of this, rods of the same size have different absorption maxima in different solvents. Figure 3 shows the experimental spectra of the GNRs in different solvents as well as correlation between the refractive index and the longitudinal SPR peak maximum. Figure 3 states that when refractive index near the nanoparticle surface increases, the nanoparticle absorption spectrum shifts to longer wavelengths.

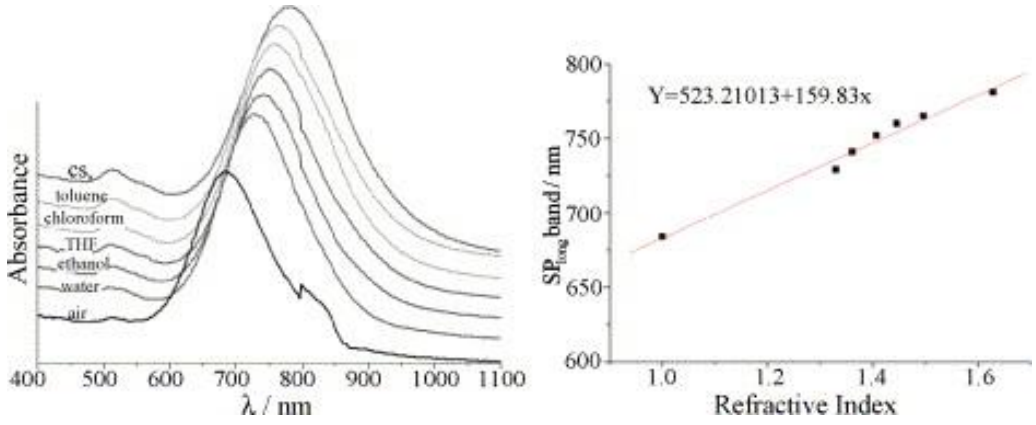

Figure 3. *Experimental UV-Vis-NIR spectra of GNRs in different solvents (left) and change in the longitudinal plasmon band position with refractive index of the solvent (right) [12].*

2.2 Photothermal effect of the gold nanorods

Gold nanorods can convert electromagnetic energy into heat via process called photothermal effect. When the GNRs are exposed to light with a wavelength close to the longitudinal SPR of the rods, the rods absorb light effectively. Rods can then convert the absorbed light into heat via a series of non-radiative processes. At the beginning of the energy transformation process, electron-electron collision quickly leads to phase loss of the coherently oscillating electrons. This phenomenon produces hot electrons with temperatures as high as 1000 K. Then the electron transfers the energy to the phonon by electron-phonon interactions. The lattice temperature can increase a few tens of degrees. These interactions are extremely fast: the electron-electron interaction occurs within femtoseconds and the electron-phonon interactions within picoseconds. [11]

Thermal energy, that was stored in the metal lattice, can be released to three different processes. Firstly, the most important process for applications is that the lattice is cooled by transferring heat to the environment via phonon-phonon interactions. Therefore, the environment heats up. This occurs within hundreds of picoseconds. Secondly, if too much heat is generated to the lattice, it can melt. The third option is ablation, where matter is vaporized on the surface of the material. [11]

The heat-releasing factor of GNRs can be utilized, for example, in biology in the form of destruction of cancer cells [5]. The amount of light absorbed by the rods is on the average 5-6 times higher than that of the best organic dye [11]. Due to this feature, the GNRs are also good alternatives also for fabrication of photoactuated materials.

2.3 Synthesis of gold nanorods using seed-mediated growth method

Gold nanorods may be synthesized in many different ways but the most common methods are seed-mediated and electrochemical growth methods [5]. In this work, the rods are synthesized using the seed-mediated growth method, which was chosen because it is relatively simple, GNRs can be produced in high yield and the aspect ratio can be easily modified [8]. The selected method can be used to produce rods with a longitudinal plasmon resonance at about 600-850 nm wavelength corresponding to an aspect ratio of 2-4.5.

As the name indicates, this method starts with **gold seeds.** Gold seeds are prepared by the reduction of gold(III) chloride trihydrate ($HAuCl_4 \cdot 3H_2O$) with sodium borohydride ($NaBH_4$). Sodium borohydride is a strong chemical reductant, which reduces the Au(III) ions directly into metallic gold. Thus, small 5-7 nm spherical gold nanoparticles are formed, which serve as the starting point for the GNRs growth. Usually surfactants must be used in synthesis of GNRs. A surfactant binds to the surfaces of the rods and prevents

their aggregation. In this synthesis, hexadecyltrimethylammonium bromide (CTAB) is used as a surfactant. [7]

For the synthesis of the actual rods, **a growth solution** is prepared. In addition to CTAB and the gold salt, the growth solution also contains silver nitrate, which acts as a catalyst. Instead of sodium borohydride, ascorbic acid is used for reduction. Ascorbic acid is a weak reducing agent and it reduces the Au(III) ions to Au(I) ions. After adding a small amount of seeds into the growth solution, gold ions are reduced on the surface of the seeds and the gold particles grow into a rod shape. Aspect ratio of the rods can be easily controlled, for example, by changing the amount of gold or silver ions in the solution [8]. Figure 4 presents a schematic diagram of the synthesis steps. Synthesis yield can be improved and the size distribution narrowed down using a small amount of additives. For example, salicylic acid derivatives can be used as additives [15].

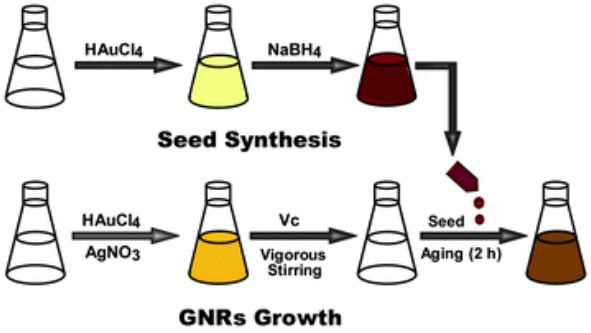

Figure 4. *Schematic picture of GNR synthesis with seed-mediated growth method. Firstly, seed solution is prepared, after which it is pipetted to the growth solution [16].*

GNR synthesis requires both thermodynamic and kinetic control that increases the number of parameters that should be taken into account. For example, temperature has a large influence on the success of the synthesis. Other important parameters are the length and width of the rods, aspect ratio, reduction yield, how much gold ions are reduced, and shape yield. For comparison, spherical gold nanoparticles can be described by just the average diameter. [15]

2.4 Mechanism of gold nanorod growth

The growth mechanism for gold nanorods is not yet fully understood [10]. Achieving an anisotropic growth is the sum of many factors and its research and understanding has proven to be quite a difficult task. However, mechanism of the anisotropic growth of the GNRs is based on reduction of the gold from $HAuCl_4$. In the growth of GNRs, three different oxidation states of gold are involved: Au(III) in the precursor, Au(I) as an intermediate, and Au(0) that forms the actual nanoparticle [15]. The first step of the mechanism is that Au(III) ions are reduced to Au(I) because of the ascorbic acid. After that, two

mechanisms have been proposed. According to one theory, disproportionation reaction of metallic gold is obtained when Au(I) ions react to the Au(0) and Au(III) ions:

$$3\mathrm{Au(I)} \rightarrow 2\mathrm{Au(0)} + \mathrm{Au(III)}. \quad (1)$$

Au(III) ions are reduced again immediately to Au(I) ions due to the reducing effect of ascorbic acid. Another theory is that the seed particles "pull" electrons from the reducing agents, thereby receiving an excess of electrons [15]. Thereafter, Au(I) ions can be reduced on the surface of the seeds.

Silver ions have considerable importance in understanding the reaction mechanism. The reaction mechanism is different depending on whether or not silver ions are used in the synthesis or not. Silver ions cannot be reduced to metallic silver in acidic reaction conditions if ascorbic acid is used as a catalyst [12]. However, silver ions can still reduce on a gold metal substrate via mechanism known as underpotential deposition [10]. The deposition of silver onto the gold surface can happen at lower potential and is expected to occur more readily on the sides of the rods compared to the ends of the rods. Thus silver prevents the reduction of gold at the sides of the rod because that would require re-oxidation of silver. This enables the anisotropic growth of the gold particles [10]. The effect of silver ions has also been shown in different theories. According to Murphy *et al*. [4], silver ions form a silver bromide solution with bromine, which is then adsorbed in a different way to the ends and sides of the rods.

2.5 Chemicals used in the synthesis

This section introduces the chemicals used in the gold nanorod synthesis. In addition, this section presents how the aspect ratio of the rods can be tuned with a change in the amount of these chemicals.

2.5.1 CTAB as a surfactant

The surfactant used in the synthesis of gold nanorods plays a major role in the growth mechanism. Today, the most common chemical that is used as a surfactant is hexadecyltrimethylammonium bromide (CTAB) [10]. When CTAB dissolves in water, it consists of two ions: the actual surfactant and the bromide ion (Figure 5). CTAB is an amphiphilic molecule that has both polar and non-polar ends and therefore it forms micelles in an aqueous solution. CTAB tends to form rod-shaped micelles (Figure 5), which together with the silver ions guide the anisotropic growth of GNR [17]. CTAB also affects also the reduction of the gold ions, because it forms complexes with gold ions and modifies their redox potential so that the reduction can occur [10].

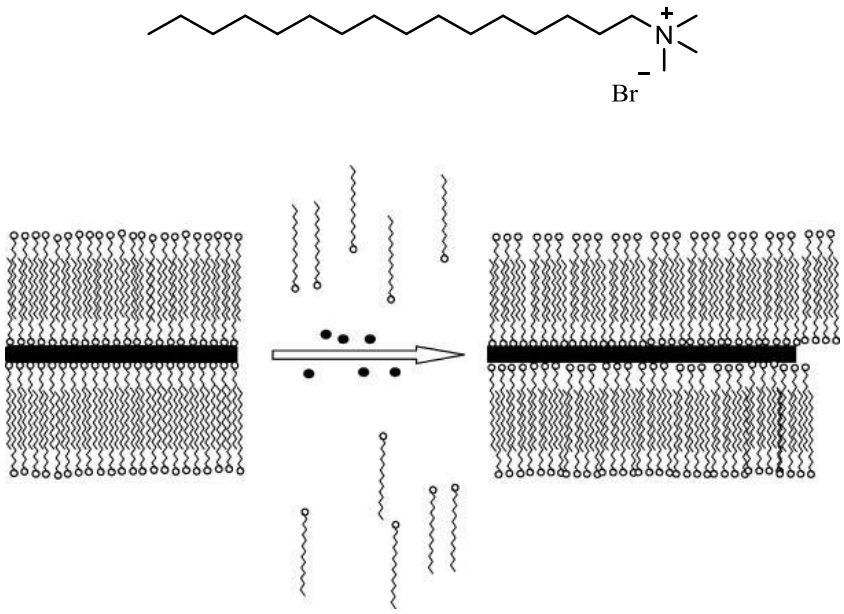

Figure 5. *Structural formula of CTAB (top) and schematic picture of formation of CTAB-bilayer to the surface of the GNR (bottom) [18].*

CTAB has a critical micelle concentration of about 1 mM [19]. Below the critical micelle concentration, micelles are not formed. However, in the synthesis of GNRs, CTAB concentration of about **0.1 M** has to be used [18]. The yield of the synthesis drops dramatically, if the CTAB concentration is reduced below 0.1 M, because stabilization effect of the CTAB deteriorates [7]. On the other hand, a large amount of CTAB is difficult to remove from the solution at the purification stage. This is why change in concentration of the CTAB to tune aspect ratio is not a good choice [7].

2.5.2 Effect of amount of gold and silver in controlling aspect ratio

The aspect ratio of the gold nanorods, and consequently the location of the longitudinal SPR peak, can be controlled effectively by changing the amount of gold or silver salt used in the synthesis. This is illustrated in Figure 6: increasing the amount of $AgNO_3$ or $HAuCl_4$ increases the aspect ratio of the rods up to a certain point. After this point, however, the aspect ratio begins to decrease in both cases. Optimizing the silver and gold ion concentrations, the longitudinal SPR band maximum of GNRs can be extended to about 850 nm, which corresponds to an aspect ratio of 4.5 [8]. The amount of the gold salt also affects also the final concentration of the rods. By increasing the amount of gold salt, the rod concentration can be increased [7].

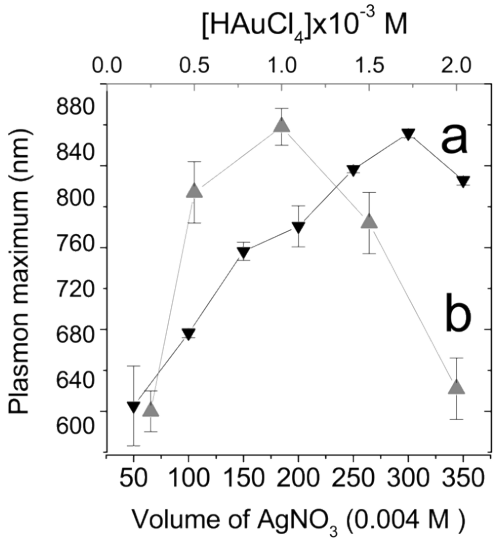

Figure 6. *Increasing the concentration of silver ions (a) first increases and then decreases the aspect ratio of the GNRs. Similar trend is also observed also for $HAuCl_4$ (b) [8].*

2.5.3 Seeds

Preparation of the seed solution is a critical step in the synthesis of the GNRs. A high-quality seed solution is necessary to obtain high-quality GNRs [15]. The amount of seeds in the solution affects the aspect ratio of the GNRs. When the amount of seeds is increased, the aspect ratio of the rods is reduced [7]. This is because there are less gold ions per one seed particle that can be reduced on the surface of the seed.

2.5.4 Ascorbic acid as a reductant

Ascorbic acid is the most popular reducing agent used in seed-mediated growth of GNRs [15]. The size and aspect ratio of the GNRs can also be controlled by the amount of ascorbic acid. The more ascorbic acid is added, the shorter rods can be obtained. If ascorbic acid is added to a large excess, no rods are formed because too much reduced gold overwhelms the growth process and leads to other shapes than rods [7].

2.5.5 5-bromosalisylic acid as an additive

Additional chemicals can be used in the synthesis process to improve the shape and size dispersion of the rods. In particular, salicylic acid and its derivatives are in common use nowadays [15; 17]. Because additives promote the micellization of CTAB, the concentration of CTAB can be reduced by a factor of two. This reduces the material costs of the

synthesis but also offers the benefit of fewer washing steps that are necessary for purification [17]. In this work, the GNRs were synthesized by using 5-bromosalisylic acid as an additive.

The addition of 5-bromosalisylic acid also has also an impact on the aspect ratio of the GNRs. Namely, the aromatic additives can also reduce the Au(III) ions to Au(I) ions. This can be used as a "pre-reduction" step to adjust the aspect ratio. The more gold ions are pre-reduced by the additive, the shorter rods are formed [20]. Pre-reduction can be monitored using a UV-Vis spectrometer. Because CTAB-Au(III) absorbs light at 396 nm but CTAB-Au(I) complex does not, this wavelength can be used to track off how many gold ions are being pre-reduced [20].

2.6 Characterization of gold nanorods

The main techniques required for GNR characterization are **UV-Vis-NIR absorption spectroscopy** and **transmission electron microscopy (TEM)** [15]. Figure 7a presents what kind of information can be achieved from the UV-Vis-NIR spectrum. Size dispersion of the GNR solution can be estimated from the full width at half maximum (FWHM) of the absorption peak related to the longitudinal SPR. The lower the value of the FWHM, the narrower the size dispersion is. Estimation of the size dispersion can also be made by checking the shape of the longitudinal SPR band, because rods with different size and aspect ratio absorb light in different wavelengths and with different magnitude. If the band is symmetric, it means that the size dispersion is narrow.

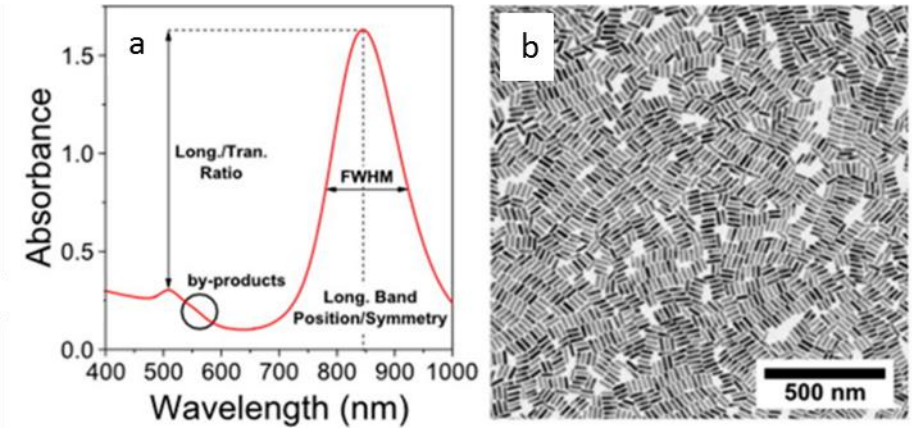

Figure 7. *a) Typical UV-Vis-NIR spectrum of GNR solutions and b) TEM image of the GNRs [15].*

The aspect ratio can be estimated from the maximum absorbance wavelength of the longitudinal SPR band, by using the relation between the aspect ratio and the band maximum given in Figure 2. The presence of byproducts, for example spherical and square-shaped particles, can be estimated from the shoulder on the transverse SPR peak maximum as Figure 7a states. On the other hand, a transmission electron microscope image (Figure

7b) gives complementary verification for the particle dimensions, aspect ratio and the presence of byproducts. UV-Vis-NIR spectrum and TEM complement each other and both of them should be used during the characterization process [15].

2.7 Concentration of gold nanorod solution

For further applications, it is important to know the concentration of the gold nanorods in the solution. Rough estimation of the concentration can be made using UV-Vis-NIR spectrum and Lambert-Beer law [15]:

$$A = c\varepsilon b, \tag{2}$$

where A is the absorbance at a particular wavelength, c is the concentration of the absorbing units in the solution, ε is the molar absorption coefficient, and b is the optical path length of light travelling in the sample (*i.e.* width of the cuvette). The absorbance at a given wavelength can be determined from the UV-Vis-NIR spectrum. Murphy *et al*. [13] have identified a relationship between the molar absorption coefficients and longitudinal SPR band maximum wavelength (Figure 8), using the same synthesis method that has been used in this work. Longitudinal SPR band maximum wavelength can be determined from the measured UV-Vis-NIR spectrum and molar absorption coefficient can be determined from the data provided by Murphy *et al*. [13]. Finally, because the cuvette width is known, Lambert-Beer law can be used to determine the rod concentration. Depending on the source, the concentration can either be presented in the unit mol l^{-1} or rods per liter. The conversion between the units can be done by using the Avogadro constant ($6.022 \cdot 10^{23}\,mol^{-1}$)

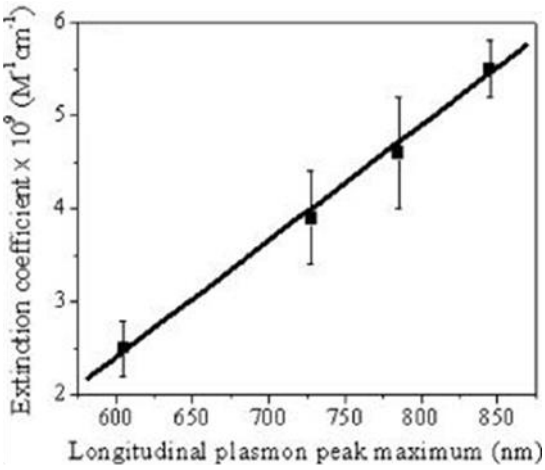

Figure 8. *Plot of absorption coefficient versus longitudinal plasmon resonance peak maximum for GNRs with the aspect ratios from 2.0 to 4.5 [13].*

The method described above is not very accurate, which can be seen, for example, from the large error limits of the graphs. However, this method can be used to assess the magnitude of the concentration of the rod solutions. A more accurate determination of the

concentration could be made by inductively coupled plasma atomic emission spectroscopy. However, such a device was not available for this Thesis work.

2.8 Functionalization of gold nanorods

Gold nanorods are often synthesized in water using CTAB as a surfactant. In this case, the shape, size and aspect ratio of the rods can be controlled efficiently [21]. CTAB-coated nanoparticles are soluble in water and poorly soluble in organic solvents. In this work, the target is to dope the GNRs into a mixture of liquid-crystalline compounds that are then polymerized to form an LCE. To achieve uniform and controlled photothermal actuation through GNR surface plasmon absorption, the nanoparticles must be well dispersed within the organic LCE matrix [22]. Therefore, rods must be functionalized so that they are soluble with organic medium provided by the liquid-crystal elastomers.

For a successful phase transfer, the nanorods are coated with molecules that are soluble in organic solvents. There are several strategies how to functionalize GNRs but layer-by-layer technique and **ligand exchange reactions** are the most popular methods [23]. In the layer-by-layer method, the whole GNR including CTAB is coated with polymer layers. The first layer is made using a negatively charged polyelectrolyte that covers the positively charged CTAB bilayer. Each successive layer is a polyelectrolyte with opposite charge and the layers are held together by electrostatic interactions [24]. For example, polyethyleneimine is one molecule that can be used in layer-by-layer technique. However, GNRs functionalized with layer-by-layer techniques are not very stable [24]. Therefore, in most cases ligand exchange method is the preferable choice. In ligand exchange reaction, molecules must be able to replace the CTAB molecules on the surface of the rods [23]. Organic molecules containing thiol, amine or carbonyl groups can be used in the ligand exchange reaction as they have high affinity to gold. The new ligands must have higher affinity to the surface of the GNR so that they can displace the CTAB bilayer. The ligand exchange reaction must also be rather quick so that the rods have no time to aggregate [25]. Thiols are often preferred, since they can form relatively strong semi-covalent gold-sulfur bond on the gold surface. This bond strength is about 190 kJ mol^{-1} which is notably higher than the electrostatic interaction between CTAB and gold [23].

In this work gold nanoparticles are functionalized using poly(ethylene glycol) methyl ether thiol (mPEG-SH) and dodecanethiol (DDT). Structural formulae of these molecules are given in Figure 9. Dodecanethiol has a long non-polar carbon chain, which makes it well soluble in organic solvents such as chloroform. Dodecanethiol has one thiol group (-SH), which allows it to bond tightly to the surface of the GNR [23]. Thanks to the tight bond, the phase transfer can often be performed relatively quickly (during 1 hour).

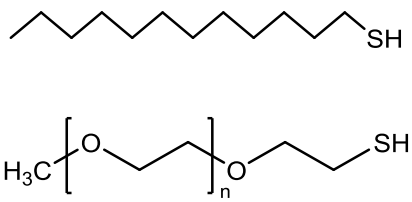

Figure 9. *Structural formulae of the chemicals used in functionalization of GNRs: dodecanethiol (up) and poly(ethylene glycol) methyl ether thiol (bottom).*

However, if only dodecanethiol is used, aggregation of the particles often occurs [21]. This can be seen at least in large (> 20 nm) nanoparticles [26]. To prevent aggregation, GNRs can be first pre-coated with the thiolate polyethylene glycols. mPEG-SH binds to the surface of the GNR by the thiol group, and its long carbon chain prevents aggregation of the nanoparticles during the phase transfer [26]. mPEG-SH is soluble in both water and organic solvents, which helps the functionalization [26]. Thiolated polyethylene glycols are commercially available in several different molecular weights and structures. After pre-coating with mPEG-SH, the rods are easier to coat with dodecanethiol. Figure 10 shows a schematic picture of this coating strategy.

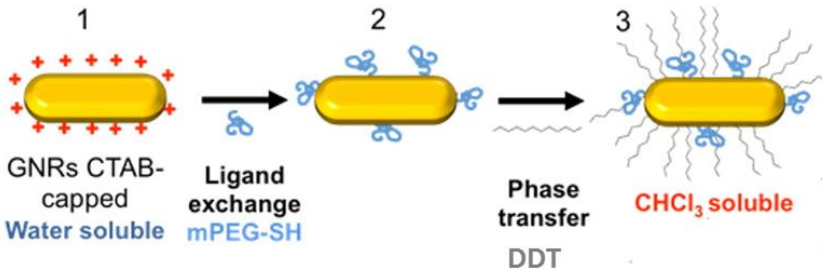

Figure 10. *Schematic picture of the coating strategy with mPEH-SH and DDT. 1) Rods are coated with CTAB double layer and they are water soluble. 2) Rods are coated with mPEG-SH polymer. 3) Rods are coated with DDT and they dissolve into organic phase. Adapted from Ref. [26].*

3. LIQUID CRYSTALS AND LIQUID-CRYSTAL ELASTOMERS

Liquid crystals consist mostly of rod-like organic molecules that tend to self-organize and align in the same direction [27]. Liquid-crystal elastomers, on the other hand, are loosely cross-linked polymer networks constituting the liquid-crystal moieties as part of the network, and sometimes as dopants as well [2]. In this chapter, theories behind liquid crystals and liquid-crystal elastomers are briefly discussed, followed by a description of actuation of LCE materials.

3.1 Thermotropic liquid crystals

Liquid-crystal displays are by far the best-known application of liquid crystal [28]. The displays are based on the light-modulating properties of liquid crystals and are used, for example, in televisions and mobile phones. However, besides the well-known display technology, there are also many other applications, such as polarized-light-reflecting materials and spatial light modulators, where liquid crystals are of great potential [29].

Liquid crystals have properties that are intermediate to those of solids and liquids. Liquid-crystal molecules can self-organize, *i.e.*, possess a certain degree of order such as that in solid crystalline materials, but they are still soft, even liquid, and thereby characterized by high mobility. In the case of thermotropic liquid crystals, phase transitions between crystalline, liquid crystalline, and isotropic phase, occur because of a change in the temperature. In such materials, the liquid-crystal phases occur below the melting point of the substance above which it turns into an isotropic liquid (Iso), but at temperatures higher than those at which the substance is a crystalline solid (Cr). For this reason, the liquid-crystalline phases are often times called mesophases. Every liquid crystal or liquid-crystal mixture has its own characteristic phase-transition temperature, depending on its chemical nature. [29]

Thermotropic liquid crystals are divided into two categories: **nematic (N) and smectic (Sm) phases**, which are distinguished by their different self-organization and optical properties (such as birefringence). A liquid-crystal material can exhibit both of these phases, or just one of them. The nematic phase is the most common and the least ordered LC phase [30]. Molecules have no positional order, but they self-align to have long-range orientational order. The molecules can move past each other easily, but they still retain the same orientation [27]. The order in this type of LC phases is based on a rigid and anisometric, in most cases rod-shaped or disc-shaped, molecular structure. In smectic phase, which is found at lower temperature than the nematic phase, there exists molecular layers that can move relative to the other layers [27]. Smectic phases can be divided into

several sub-phases according to how the molecules are oriented with respect to the layers' normal. In smectic A phase (SmA) molecules point to the same direction as the layer normal, whereas in smectic C phase (SmC) molecules are tilted away from the normal direction [30]. Figure 11 illustrates the molecule order of the different LC phases.

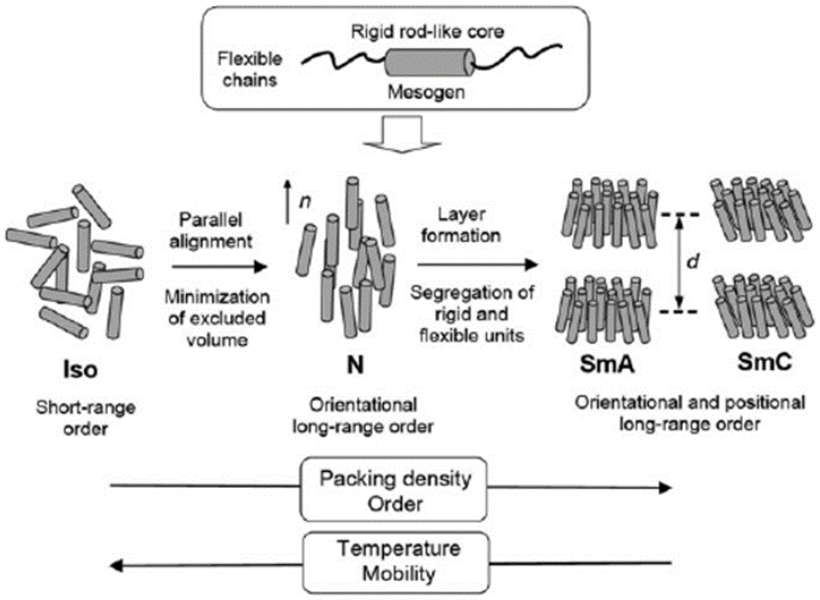

Figure 11. *Organization of rod-like molecules in different LC phases. In the isotropic phase, molecules have no regular organization. In the nematic phase, the molecules point to the same direction and in the smectic phase there are regularly arranged layers [29].*

Organic molecules that can form liquid crystals are sometimes called **mesogens**, "meso" referring to properties that are intermediate to those of solids and liquids. The most typical forms of mesogens are rods, laths, discs, and helices. In this work, rod-like mesogens are used. Figure 12 shows the structure of a typical rod-like liquid crystal molecule. Two phenyl rings and a linking group between them confer a rigid structure. The chemical stability of liquid crystals depends strongly on the central linkage group. The side chain is commonly a hydrocarbon chain that serves to elongate the molecule. The side chain of the liquid crystal molecule influences, for example, the transition temperatures of the liquid crystal phases. The terminal group is often polar, giving rise to intermolecular attractions along the long axis, and it affects anisotropy of the liquid-crystal. The polarity of the mesogen is an important property, because it allows for, for example, the orientation of the mesogens to be controlled with electric field. [27]

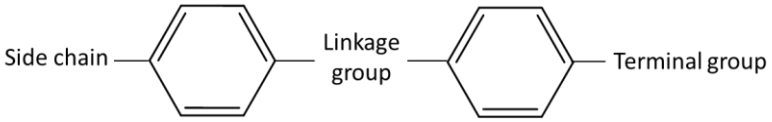

Figure 12. *Rod-like LC molecule consists of two or more benzene ring systems connected by a linkage group.*

3.2 Order parameter of the nematic liquid crystals

Liquid crystals have long-range orientational order, which is their most defining feature. Because of this order, the physical properties of LCs are anisotropic [27]. The order parameter (S) of the liquid crystals expresses **how much orientational order is present in the material**. It can be defined by the following equation [31]:

$$S = \frac{1}{2} < 3\cos^2(\theta) - 1 >, \qquad (3)$$

where θ is the angle between the local director (**n**) and the long axis of each rod-shaped liquid crystal molecule (see Figure 13a), and the brackets denote averaging over all the molecules. The local director is defined to be the average direction of the molecular long axes in the LC phase. The individual rod-shaped molecules are generally tilted with respect to the local director because of thermal fluctuations [32].

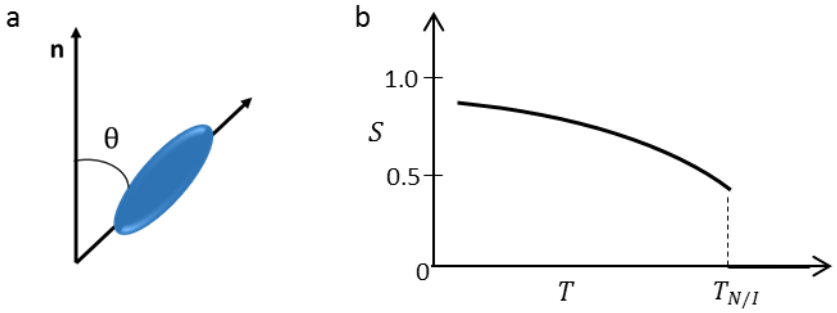

Figure 13. *a) Schematic picture showing angle between local director and LC molecule and b) typical temperature dependence of the nematic order parameter.*

For nematic liquid crystals, the order parameter is typically between 0.3 and 0.7 [32]. For a perfectly ordered material, the order parameter is one, while in an isotropic liquid it is zero. Typical temperature dependence of the nematic order parameter is presented in Figure 13b. The order parameter decreases when the temperature increases and at the nematic-isotropic transition temperature ($T_{N/I}$) it falls to zero.

3.3 Liquid-crystal elastomers

Liquid-crystal elastomers are materials which have properties of both liquid crystals and elastomers: the self-organization nature of liquid crystals and the flexibility of the polymeric network [30]. LCEs exhibit coupling between anisotropic molecular order because of the presence of LCs, and elasticity brought about by the polymer network. The most important feature of LCEs is that they can **change their shape reversibility in response to an external stimulus**. The external stimulus may be a change in temperature, electric or magnetic fields, or electromagnetic radiation [30]. A change of the orientational order of the mesogenic units by external stimuli results in a change of the polymer backbone conformation and therefore the macroscopic shape of the LCE [33]. In LCEs, the mesogens are directly attached to the elastomeric polymer network, to yield a main-chain elastomer or a side-chain elastomer [28]. Figure 14 illustrates these two different types of LCEs. Connectivity of the mesogenic group can affect the architecture of the LCE network. The mesogenic group can be attached to the polymer chain either longitudinally (as in Figure 14) or transversely.

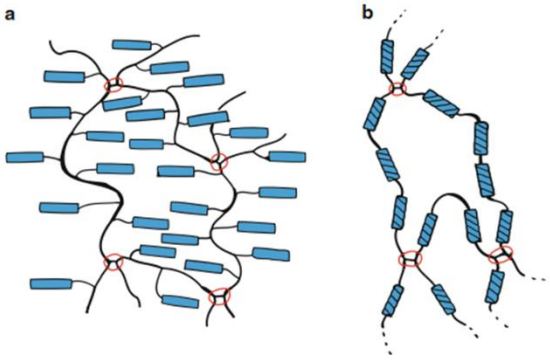

Figure 14. *(a) LCE network containing side-chain mesogens; (b) LCE network containing main-chain mesogens [28].*

One of the main factors affecting the properties of the LCE is cross-linking density. LCEs have relatively low cross-linking density, which makes them soft and flexible. This means that they can undergo large changes in order and shape when subject to even a relatively weak external stimulus. When cross-linking density is increased, LCEs lose their flexibility. When this happens, the material is called liquid-crystal polymer network (LCN) rather than an elastomer [34]. Distinguishing in the cross-linking density between LCE and LCN is not easy but it can be done considering Young's modulus [34], which measures the ability of a material to withstand changes in its shape under stress [35]. Typical Young's modulus is in the order of megaPascals in LCEs and gigaPascals in LCNs. High cross-linking density is needed for the generation of high mechanical force. High deformations, on the other hand, benefit from low cross-linking density [28].

Liquid-crystal elastomer is prepared by synthesizing long polymer chains that contain the mesogens. These polymer chains are cross-linked to one another at certain positions [30].

Two main polymerization methods are **thermal and photopolymerization**, which are illustrated schematically in Figure 15. Thermal polymerization is typically based on silicon chemistry. All the starting materials are mixed at the same time and the reaction takes place on the surface of a catalyst in two steps with heating [36]. In photopolymerization method, the liquid crystal monomer is mixed with radical- and cross-linker molecules. Cross-linker molecules may or may not be liquid crystalline. Light-absorbing dyes, which may or may not take part in the polymerization reaction, can also be added. Photopolymerization occurs when the sample is irradiated with light, with a wavelength depending on the photoinitiator used, and photoinitiator decays into radicals. Then, these radicals react with carbon-carbon double bond to begin chain-growth polymerization process. The advantage of this method is that the LCE molecules can be oriented easily before the polymerization process (see Section 3.4.2). In addition, the method is quite easy and fast to implement [30].

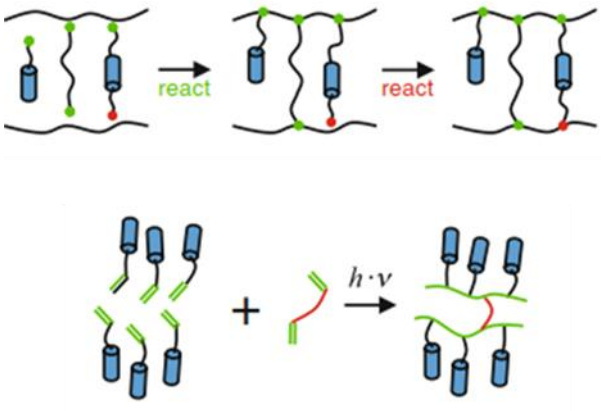

Figure 15. *The two main polymerization methods to fabricate LCEs: thermal polymerization (top) and photopolymerization (bottom). Adapted from Ref. [28].*

3.4 Photo actuation of the LCE materials

An actuator is a system that converts energy from an input stimulus into mechanical motion. In order to effectively translate the molecular-level motions into macroscopic actuation, the molecules must act in concert [4]. Concerted motions require a certain degree of internal order within the material system, which is achieved by LCE matrix. The actuation in LCEs is conventionally driven by temperature. However, considering applications, it is very impractical and often impossible to trigger the actuation process by heating the whole sample, so it would be better to use a stimulus that can be localized, applied remotely and switched on and off rapidly [37]. Therefore several different types of materials with alternative actuation stimulus, such as electric field, magnetic field, and light, have been explored [30].

In this work, LCE materials are fabricated so that they can be actuated with light. When an LCE is actuated with light, it must contain components that absorb electromagnetic radiation. Light is in many ways an ideal stimulus by being an endless and clean energy source. Its properties (wavelength, intensity, polarization) can be precisely manipulated. Finally, light stimulus can be activated remotely, and it is in most cases non-damaging to the material system. Photoactuated materials have one big advantage over the materials actuated with heat, electric or magnetic fields. These materials can serve as the main driving parts of light-driven actuators and do not need the aid of batteries, electric wires and gears [3].

Many of the observed photoactuation properties and phenomena in LCE materials result from the special coupling between the mesogens and the polymer backbone [3]. Actuation strength depends firstly on the architecture of the LCE material (see Figure 14). The main-chain elastomers, where the mesogens are attached longitudinally to the polymer backbone, have the strongest shape-change capability [2]. This is due to the strong deformation of the polymer chain conformation which affects the shape conformation. Secondly, cross-linking density and chemical nature of the LCE affect the actuation strength. Thirdly, properties of LCEs depend on the alignment order, *i.e.* order parameter, of the LC mesogens. Finally, concentration of the photoactive molecules in the LCE matrix can influence the properties of the LCE material. Concentration has to be sufficiently high to achieve good absorption. However, overly high dye concentration can weaken mechanical properties of LCE. High absorption of the film can also prevent light to penetrate through the whole film thickness and thereby change the actuation properties [3].

3.4.1 Actuation mechanism of thermotropic LCE

Liquid-crystal elastomers may exhibit large dimensional changes upon LC-to-isotropic phase transition, whereas the initial state is restored upon reverse transition due to the "memory effect" brought about by the cross-links within the LCE matrix. Nematic LCEs have the ability to reversibly actuate during phase transitions from nematic-to-isotropic phase triggered by external stimulus [38].

When LCE materials are actuated, external stimulus causes **the thermal phase transition** of the material. Phase transition provides the change in the degree of alignment of the mesogenic molecules. In the nematic phase (left in Figure 16) the polymer chains of LCE elongate when the mesogens orient along the director, whereas in the isotropic phase (right in Figure 16) they recover a random-coil conformation, which is driven by entropy [34]. This results in spontaneous elongation or contraction of the whole network along the director [28]. Therefore, when the phase transition of the nematic LCE occurs, order is changed, and the macroscopic uniaxial contraction (or restoration) of the nematic LCE along the director axis occurs [3].

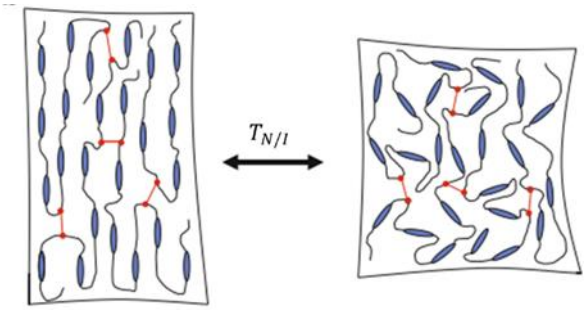

Figure 16. *Visualization of change of order at the nematic-isotropic phase transition temperature [28].*

Nematic-to-isotropic phase transition can be achieved in many ways. First, the most traditional option is to heat the material above the nematic-to-isotropic phase transition temperature. Second, if the LCE is made conductive, for example with carbon black, shape change can be achieved by applying an electric current through the sample. Electric current increases the temperature of the material, through Joule heating [28]. Third, magnetic fields can also be used to heat an LCE sample. LCE can be doped with magnetic nanoparticles after which changing magnetic field causes continuous reorientation of the magnetization which produces viscous heat and induces a shape change [30].

In the case of light actuation there are **two possible mechanisms, based on either photochemical or photothermal effect**. Photochemical effect is mostly based on photochromic molecules (such as azobenzenes), which can reversibly change their shape upon light irradiation. Shape change of the molecules effectively disrupts LCE order and allows for isothermal transition from nematic-to-isotropic phase upon light activation [4]. Another route towards light-induced actuation of LCEs is to employ photothermal effects in which case the LCE contains dyes or nanoparticles that absorb light and convert photon energy into heat. Heat is released to the LCE matrix and it induces the LC-to-isotropic phase transitions and the shape change. Competition or collaboration between these two mechanism is not yet fully understood [37].

3.4.2 Modes of actuation

The main modes of the actuation are **contraction, expansion and bending**. Alignment of the LC molecules strongly affects the actuation modes. In LC-cell alignment method, LC molecules can be aligned in several ways [39]. Boundary conditions can be controlled using polymer-coated glass substrates. For example, polyimides can be used as coating materials. Moreover, rubbing of the polymer coating on the glass substrate can be used to direct the alignment. Figure 17 shows the three main alignment schemes of the LCEs: homogenous (called also planar), homeotropic, and splay. In a homogeneously aligned cell, the LC molecules are parallel to the bounding surfaces and point to the in-plane direction. In the homeotropic alignment, the director of the LC molecules is perpendicular

to the cell walls. The alignment in these two configurations can be accomplished by coating substrates for the cell walls using different special polymers and rubbing [39]. In splay orientation molecules are tilted gradually between horizontal and vertical direction. Splay alignment can be achieved by placing two different alignment layers on top of each other while preparing the liquid-crystal cell.

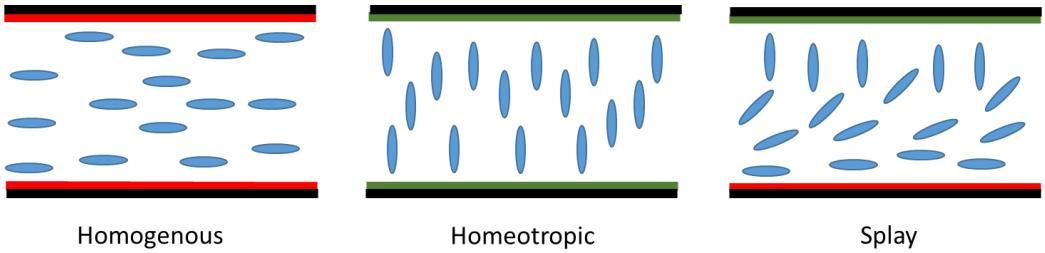

Figure 17. *Schematic picture of the mesogen orientation in nematic phase in different boundary conditions.*

Homogenous or homeotropic samples can undergo both contraction-expansion or bending, depending on the structure of the LCE. In these films bending can also occur because of the temperature gradient inside the films. However, in splay-oriented LCE films bending is the main actuation mode. This is because the two sides of the film are distinct from one another. When splay-oriented films are actuated, the homeotropically aligned side tends to expand and the homogenous side contracts at the same time. As a result, bending occurs.

3.4.3 Photo actuation of LCE based on azobenzenes

The most popular photochromic molecules that are used in light-actuated LCE materials are the aromatic azobenzene derivatives in which two phenyl rings are bridged by an azo (–N=N–) linking group [3]. Azobenzenes absorb light strongly in the UV to visible red region, depending on the ring substitution [40]. All azobenzene derivatives can undergo reversible **photoisomerization** between a thermally stable *trans*-state and a metastable *cis*-state when they absorb a photon, as is illustrated in Figure 18. Isomerization causes a significant change in the molecular length from about 9 Å in the *trans*-form to 5.5 Å in the *cis*-form [3]. Photoisomerization of azobenzene in its thermodynamically stable state occurs when it absorbs a photon, with a wavelength at the *trans* absorption band. Reverse *cis-to-trans* isomerization can be either light-induced or thermal. In the case of LCEs, the isomerization reaction can produce large structural changes, and generate a force that initiates macroscopic photochemical effects such as photoinduced actuation.

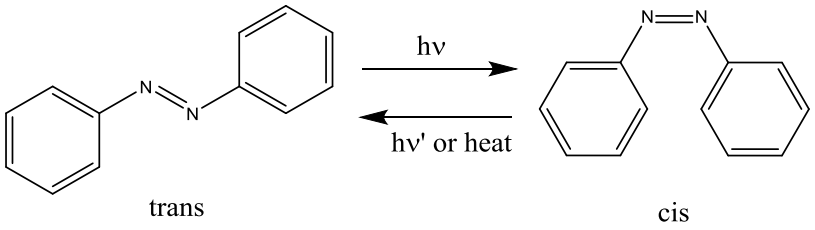

Figure 18. *Photo isomerization of azobenzene.*

Azobenzene derivatives can be simplistically divided into three classes according to their spectroscopic properties: azobenzene-type molecules, aminoazobenzene-type molecules and pseudostilbenes. The classification is based on the n → π∗ and π → π∗ molecular electronic transitions and their energies. Figure 19 shows the basic structure and absorption spectra of these different azobenzene types. The azobenzene-type molecules have a high intensity π → π∗ band in the UV region, and a low intensity n → π∗ band in the visible region. Many azobenzene derivatives, especially those substituted with non-polar groups such as alkyl or alkoxy chains, exhibit similar absorption than unsubstituted azobenzene. However, as the absorption spectra in Figure 19 state, substitution can also lead to a red-shift in the absorption maximum. In aminoazobenzenes, the parent azobenzene is *para*-substituted with an electron-donating group, for example the amino group (-NH_2), due to which the π → π∗ band is red-shifted to the wavelengths around 400 nm, rendering the n → π∗ transition less obvious. Pseudostilbenes are substituted with strong electron-donating and electron-withdrawing groups, which leads to a strongly asymmetric electron distribution that is called the push–pull effect. This effect shifts the π → π∗ absorption to the higher wavelengths past the n → π∗ transition. [41]

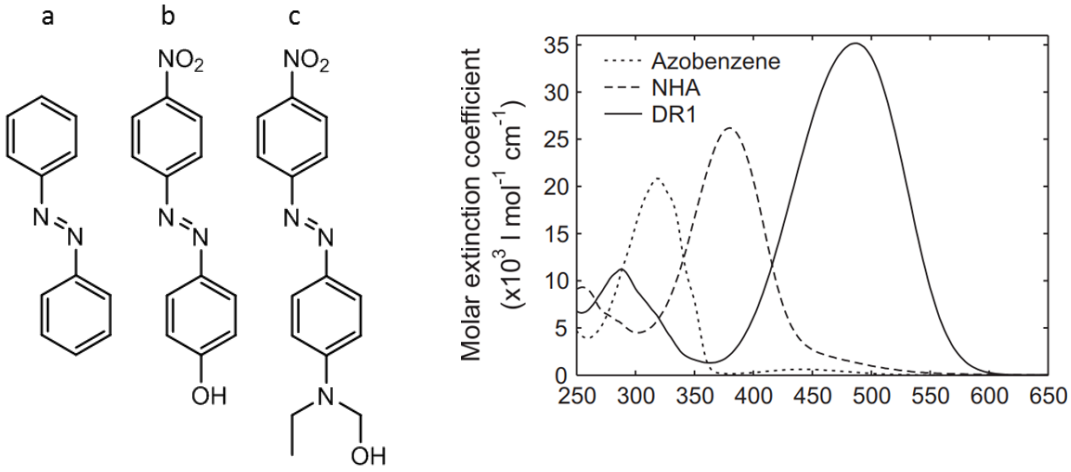

Figure 19. *Examples of a) azobenzene-, b) aminoazobenzene- (NHA) and c) pseudostilbenes-type [Disperse Red 1 (DR1)] molecules (left) and absorption spectra of these molecules (right) [40].*

Photoisomerization of the azobenzenes results in significant changes in their absorption spectrum, which is illustrated in Figure 20. The high absorption band of the *trans* π → π∗

transition is reduced and blue-shifted whereas the n → π∗ transition is more visible in the *cis*-state. The thermal relaxation times of the aminoazobenzene- (minutes) and pseudo-stilbene-type (seconds) azobenzenes are faster than those of azobenzene-type molecules (hours), making the spectra of their *cis*-forms more difficult to measure. [40]

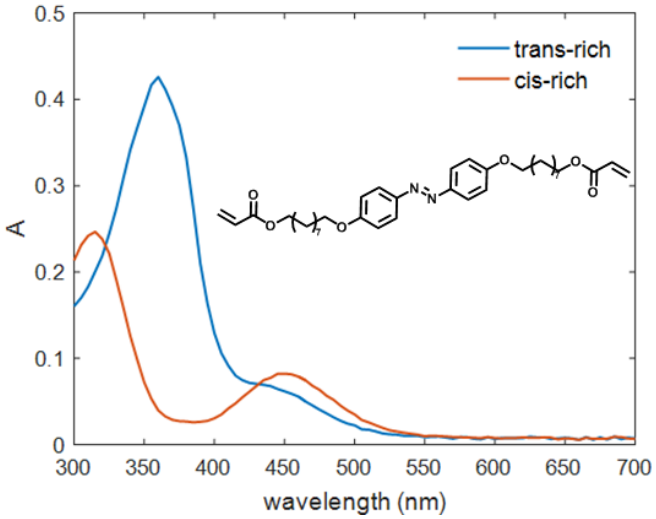

Figure 20. *Absorption spectra of the trans- and cis-rich photostationary states of 4,4'-Bis[9-(acryloyloxy)nonyloxy]azobenzene that is used in this work. The spectra are measured from $2 \cdot 10^{-5}$ mol l^{-1} chloroform solution before and after irradiating with 385 nm light from an LED.*

In LCEs, the *cis-trans* isomerization of azobenzenes can be utilized in two ways. The azobenzenes can be covalently bonded to the polymer backbone, or just doped into the LCE matrix [28]. Agreement has not been established on whether the actuation mechanism is based on photochemical, photothermal effects or combination of these two. However, common opinion is that when azobenzene is covalently bonded to the polymer backbone, *cis-trans* isomerization is the dominant mechanism [42], while in the doped azobenzene systems, both mechanism have received support [43; 44].

For utilizing azobenzene-type LCEs, UV light, which typically has relatively small penetration depth into the LCE material, must be used for actuation [22]. Furthermore, their relaxation time back to *trans*-form is long unless a second stimulus is used [22]. The latter problem can be solved by using substituted azobenzenes with absorption shifted to longer wavelengths. Usually, the thermal relaxation time is also shortened.

3.4.4 Photoactuation of LCEs based on nanoparticles

Different kinds of nanoparticles can be used to actuate LCE materials, and in fact, this concept has been of considerable interest in recent years [3; 45]. Most common nanoparticles that can be used to photoactuation of the LCE material are carbon nanotubes and plasmonic gold nanoparticles. These can **absorb light efficiently and convert it to heat fast.** Moreover, nanoparticles can absorb light in longer Vis-IR wavelengths which is

attractive for actuation because of its lower energy and deeper penetration abilities than UV light [1]. Nanoparticles can be utilized in two ways: they can be placed into a thin layer onto the LCE surface or doped homogenously into the bulk LCE [45]. In the case of doped LCE matrix, nanoparticles can be functionalized with molecules which can covalently bond with the LCE polymers [1]. Another way is to just incorporate functionalized nanoparticles into the LCE matrix without covalent bonding [22], as is done in this work.

Especially gold nanorods in LCEs are of great interest because they have large optical absorption cross section so they have good photothermal conversion efficiency as well. Because of this feature, GNRs can induce rapid shape-changing response for GNRs-LCE upon light irradiation [22]. Moreover, the aspect ratio of GNRs and therefore the actuation wavelength can be easily tuned. Finally, GNRs absorb visible light, wherein the activation of material is easy and can be done with lasers [33]. For example, Hauser *et al*. [22] have doped gold nanorods into an LCE using photopolymerization to fabricate the films. With this method, GNRs can be aligned with the molecular liquid crystal director without any additional driving forces for alignment (for example stretching, or electric/magnetic fields).

One of the main problems in the utilization of the GNRs is that they are usually difficult to disperse in organic LCE matrixes and they may weaken the mechanical properties of the matrix [46]. Furthermore, GNRs aggregate easily, thereby losing their SPR properties when they are dispersed in the LCE matrix [1]. Using large quantities of the GNRs in the LCE is particularly problematic. However, many of these problems can be solved with the proper functionalization of the GNRs.

4. MATERIALS AND METHODS

This chapter describes how the synthesis and functionalization of the materials used in this work are performed and how the LCE films containing the light-active compounds are fabricated. Moreover, this chapter describes the methods that are used to prepare and analyze the samples. Synthesis and functionalization of the GNRs and fabrication of the LCE films follows the most up-to-date and precise protocols and guidelines published in the literature.

4.1 Synthesis of gold nanorods

Because impurities affect significantly the yield and morphology of the GNRs, great care must be taken when cleaning the glassware during the synthesis process [15]. Each piece of glassware was first washed with soap and water. After this the glassware was soaked in *aqua regia*, washed with tap and Milli-Q water and finally dried. Chemicals used in GNR synthesis are listed in Table 1. Any impurities in the CTAB are very harmful to the nanorod formation. Therefore, attention must be paid to the quality of the used chemicals, especially to the purity of CTAB. As Smith *et al*. report [47] all commercially available CTAB grades are not pure enough.

Table 1. *Names, formulae, suppliers and purity of chemicals used in the synthesis of the GNRs.*

Chemical name	Formula/ Abbreviation	Supplier, (purity)
Hexadecylcetyltrimethylammonium bromide	CTAB	Sigma-Aldrich (H6269), (99%)
Gold(III) chloride trihydrate	$HAuCl_4$	Sigma-Aldrich, (99.9 %)
Sodium borohydride	$NaBH_4$	Fluka, (96 %)
Silvernitrate	$AgNO_3$	VWR (-)
L-askorbic acid	$C_6H_8O_6$	J.T. Baker (-)
5-bromosalisylic acid	$C_7H_5BrO_3$	Acros Organics (98 %)

CTAB and gold salt stock solutions are stable for long periods of time but fresh ascorbic acid and silver nitrate solutions were prepared every week [15]. Sodium borohydride releases hydrogen gas when it is dissolved in water, so a new solution was made before every seed synthesis. Gold salt, silver nitrate and ascorbic acid solution were stored in a refrigerator (4 ℃).

In this work, gold nanorods were synthesized both using an aromatic additive, 5-bromosalisalisylic acid, and without it. GNR synthesis, with or without the additive, is based on the work of Scrabell *et al*. [15]. The following synthesis protocol takes advantage of the use of additive.

Seed synthesis is performed in a water bath at 27-29 ℃. 10 ml of aqueous CTAB solution (0.1 M) was mixed with 50 µl of $HAuCl_4$ (0.05 M) and stirred gently with a magnetic stirrer for 5-10 min. Color of the solution changed from pale yellow to dark yellow. Then 0.6 ml of ice-cold $NaBH_4$ (0.01 M) was added with vigorous stirring of 900 revolutions per min (rpm) for 2 min. After addition of the $NaBH_4$, the color of the solution turned brown. It is worth noting that the stirring cannot be too hard or CTAB begins to foam and the synthesis fails. After 2 min of vigorous stirring, the seed solution was stirred gently and it was kept in a 27-29 ℃ water bath. The reaction progress was monitored by UV-Vis spectrometer. The seed solution was used for one to two hours after synthesis.

A typical **growth solution** was prepared as follows. 180 mg of 5-bromosalisylic acid was added to 200 ml of CTAB solution (0.05 M). The solution was sonicated for about 5 min so that all the additive was dissolved. Then the growth solution was placed into a 27 ℃ water bath and the temperature was allowed to equilibrate for 10 min. After that 1.4 ml of silver nitrate (0.01 M) solution was added with gentle mixing for 15 min. Then 2 ml of $HAuCl_4$ (0.05 M) was added and the solution turned dark yellow. A small precipitate was formed and dissolved quickly. The pre-reduction of gold started immediately after addition of the gold salt. The pre-reduction was monitored by a UV-Vis spectrometer at the wavelength of 396 nm. Absorbance of the solution was initially around 1.5, when the length of the cuvette was 1.0 cm, and it was allowed to decrease to 0.8, which took about 15 min. Immediately after reaching the desired value of absorbance at 396 nm, the stirring speed was increased (to about 1000 rpm) and 0.52 ml of ascorbic acid (0.1 M) was added to the growth solution. The mixture turned colorless within a few seconds. After 2 min of hard stirring, 0.32 ml of the seed solutions was added. The solution was stirred 30 s, and it was left undisturbed for at least 20 hours in the water bath at 27 ℃. Gradually, a change from colorless to red-brown solution started about 5 min after the addition of seeds.

Gold nanorods were separated from the unreacted starting materials by centrifugation. This was done 20-24 h after the addition of the seeds to the growth solution. Typically, 1.4 ml of the solution was centrifuged for 20 min at 9500 rpm. The colorless supernatant was discarded. The solid residue was re-dispersed in 0.7 ml of Milli-Q water. UV-Vis-NIR spectrum was measured before and after centrifugation. Finally, TEM pictures were taken. About 5 µL of GNR solution was dropped onto a TEM grid and allowed to dry for at least 24 h in open atmosphere.

4.2 Phase transfer of gold nanorods

Two different attempts were made to functionalize the gold nanorods. Functionalization was tried with dodecanethiol (from Sigma-Aldrich) and combination of DDT and poly(ethylene glycol) methyl ether thiol with average molar mass 6000 g mol^{-1} (from Sigma-Aldrich). Before attempting the phase transfer, GNR solutions were centrifuged one more time (20 min at 9500 rpm), and the residue was dissolved in the same amount of Milli-Q water. The tried methods are as follows:

Attempt 1 with DDT: 5 ml GNR solution was shaken for 30 min with liquid DDT (0.5 ml). GNRs were then transferred to the organic phase by the alternating addition of acetone (1 ml) and toluene (1 ml), starting with acetone. The organic phase was decanted off and the procedure was repeated until the water phase appeared colorless to the eye. Finally, because acetone is soluble in both water and toluene, the organic solution was placed into a rotavaporator (250 mbar, 30 min, room temperature) to remove any acetone from the GNR-toluene solution. [25]

Attempt 2 with 6000 g $\mathbf{mol^{-1}}$ mPEG-SH and DDT: GNRs were at first pre-stabilized with mPEG-SH. Firstly, the stock solution of mPEG-SH (15 mg ml^{-1}) in chloroform was made. This stock solution was added to the GNR solutions so that amount of mPEG-SH was 2-4 mg per 1 ml of GNR solution. The solution was shaken for 2 hours. Subsequently, a DDT solution in chloroform (1:2) was added to the aqueous phase containing the GNRs. The phase transfer was assisted by the addition of 40 µl of concentrated HCl to 5 mL of GNR solution. Phase transfer occurred after vigorous stirring for 1 h. After complete phase transfer, water was decanted off, and the organic phase was purified by centrifugation (45 min, 5000 rpm). Small amount of ethanol was added to the chloroform solution (1:5) to facilitate the precipitation process. [21]

4.3 Liquid-crystal-cell preparation

Glass cells for liquid crystals were made of Thermo Scientific microscope slides (76x26 ml). A glass plate was cut into two parts (about 30x26 ml and 46x26ml). The plates were first cleaned by sonication in 2-propanol (20 min, 45 ℃), followed by sonication in acetone (20 min, 45 ℃). After cleaning, one side of each plate was covered with a special polyimide polymer from *JSR Micro NV* by spin-coating. The plates were then heated to about 80 ℃ letting the solvent to evaporate. Finally, the plates were heated at 180 ℃ for curing the polyimide. The coating materials and parameters of the spin-coating are listed in Table 2.

Table 2. *Code of polyimide material from JSR Micro NV, spin-coating parameters and rubbing.*

Code of polyimide material	Spin-coating parameters	Rubbing
OPTMER AL 1254	1500 rpm, 1 min	Yes
OPTMER AL 60101L	5000 rpm, 1 min	no

The coated plates were rubbed with a rubbing machine (400 rpm) followed by cleaning with nitrogen gas. Dry borosilicate glass microspheres (30 μm) were used as spacers. Small amount of spacers was placed in the corners of the bigger plate and the smaller plate was placed on top of it. The top plate was pressed lightly, so that the plates set against each other uniformly. The plates were glued to each other with UVS 91 glue. The glue was cured by irradiation with 375 nm UV light (30 mW cm^{-1}) for 5 min. Cells with two different kinds of alignment were made: planar and splay. Planar cells were made by placing two AL 1254-coated glass plates against each other so that their rubbing directions were parallel to each other. Splay cell was made by placing AL 1254- and AL 60101-coated glass plates facing each other. An example planar glass cell is shown in Figure 21.

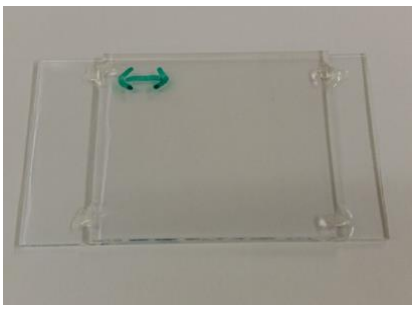

Figure 21. *A photograph of the planar glass cell. Arrow indicates the rubbing direction.*

4.4 Preparation of the LCE films

In this work, LCE films were fabricated using the photopolymerization method. Side-chain elastomers in which the mesogens are attached longitudinally to the polymer backbone (Figure 14a) were prepared. The names and structural formulae of the molecules used in the preparation of the LCE are given in Figure 22.

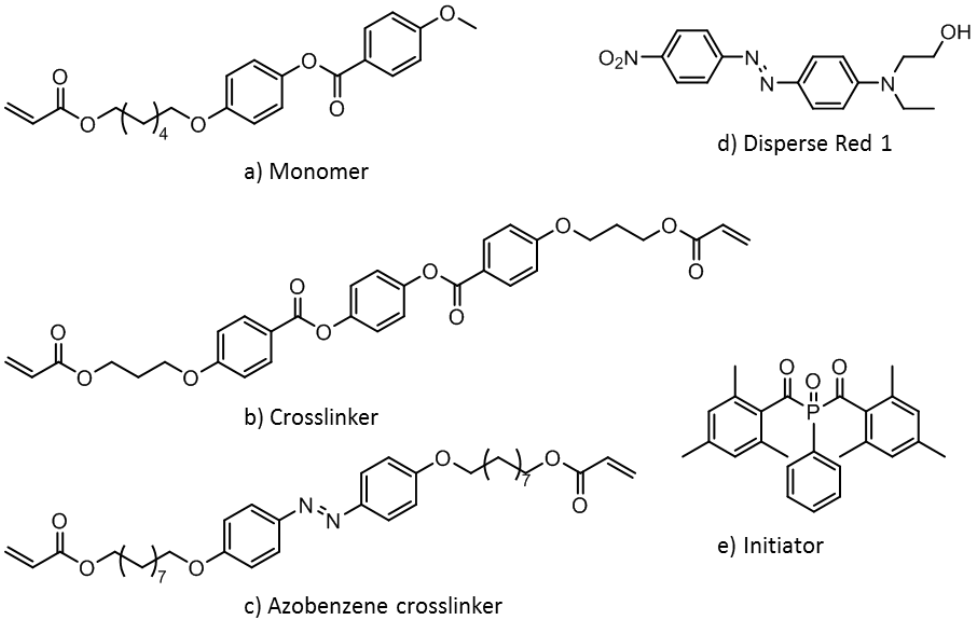

a) 4-Methoxybenzoic acid 4-(6-acryloyloxy-hexyloxy)phenyl ester

b) 1,4-Bis-[4-(3-acryloyloxypropyloxy)benzoyloxy]-2-methylbenzene

c) 4,4'-Bis[9-(acryloyloxy)nonyloxy]azobenzene

d) *N*-Ethyl-*N*-(2-hydroxyethyl)-4-(4-nitrophenylazo)aniline

e) Phenylbis(2,4,6-trimethylbenzoyl)phosphine oxide

Figure 22. *Structural formulae and names of chemicals used in the LCE film fabrication process.*

GNR-doped LCE solutions were prepared as follows: commercially available monomer (from Synthon Chemicals), cross-linker (from Synthon Chemicals) and initiator (Irgacure 819, from Sigma-Aldrich) were weighted in a glass vessel and diluted with a small amount of chloroform. After the LCE components were completely dissolved, a small amount of GNR solution was added (0.5-5 wt-% with respect to the LCE monomer). Mixtures with azobenzene cross-linker (from Synthon Chemicals) and Disperse Red 1, (from Sigma-Aldrich) were prepared similarly, but no solvent was used. From now on, these three LCEs studied are referred as **UV-LCE** (for LCE containing UV-active azobenzene cross-linker), **Vis-LCE** (for LCE containing Disperse Red 1) and **IR-LCE** (for LCE containing gold nanorods) depending on the wavelength that they absorb. All the mixtures were prepared so that mole percentage of the monomer was the same. Cross-linking density of the films and the mole percentage of the light active molecules were also kept constant. Table 3 summarizes the mole percentages of the chemicals used in LCE the film fabrication.

Table 3. *Mole percentages of the molecules used in LCE film fabrication, GNR-solutions weight percentage, and wavelength of the UV-lamp used in photopolymerization* ($\lambda_{poly.}$).

Mix	Monomer (mol-%)	Cross-linker (mol-%)	Initiator (mol-%)	Cross-linking UV-azo (mol-%)	DR1 (mol-%)	GNR (wt-%)	$\lambda_{poly.}$
UV-LCE	80.7	13	1.3	5	-	-	420
Vis-LCE	76.7	17	1.3	-	5	-	375
IR-LCE	80	18.7	1.3	-	-	0.5-5	375

After the molecules were weighted, the LCE solution was stirred with a magnetic stirrer at the temperature of about 90 ℃, which is above the melting temperature of the liquid-crystal mixtures. The solvent was allowed to evaporate from IR-LCE solution while other solutions were allowed to melt. The nematic-isotropic phase transition temperature of the mixtures was determined with a polarized optical microscope. A drop of the liquid samples was sandwiched between two microscope slides. The samples were heated to 75 ℃ after which they were cooled with cooling rate 2 ℃ min^{-1}, and the phase transition temperatures were monitored from the microscope images.

For the LCE film preparation, isotropic mixtures were cast onto the glass cells at 90 ℃. cooled to 10 ℃ below the nematic-isotropic phase transition temperature at cooling rate 2 ℃ per min, and left undisturbed for about 5 min. The cell was then exposed to 375 or 420 nm radiation (about 30 mW cm^{-1}), depending on the sample (see Table 3), for 20 min during which time the photopolymerization takes place. Primarily, 375 nm lamp was used because of better activation of the initiator. However, the used cross-linking UV-active azobenzene absorbs at 375 nm light and undergoes *cis-trans* isomerization (See figure 20). Therefore, 420 nm lamp was used when photopolymerizing this sample. After photopolymerization, the cell was opened and polarized UV-Vis spectra were measured and polarized optical microscopy studies were made for planar films. Finally, a 15 mm x 1 mm piece of the film was cut along the rubbing direction for actuation studies.

4.5 Research methods

The synthesized and functionalized gold nanorods were washed with the centrifuge and characterized with UV-Vis-NIR spectroscopy and transmission electron microscopy. In the preparation of the class cells, spin-coating and rubbing was used. The prepared LCE films were characterized with polarized UV-Vis-NIR spectroscopy and polarized optical microscopy.

4.5.1 Centrifugation

Centrifugation can be used in, for example, the solid-liquid separation process of colloids [48]. It is a simple technique that uses the centripetal force for the sedimentation of heterogeneous mixtures. Centrifugation speeds up the sedimentation process and helps in the formation of the precipitate, which would be too slow if only gravity would drive the process [48]. The remaining solution, called supernatant, may be discarded with a pipette. Phase separation time depends on many factors: particle size and shape, the concentration of the solids, and the solvent used. In this Thesis, Thermo Scientific: Sorvall ST 8 centrifuge was used.

4.5.2 Spin-coating and rubbing

Spin-coating and rubbing can be utilized when preparing glass cells for the incorporation of liquid-crystal mixtures. Spin-coating is a technique for the deposition of thin films onto a solid substrate. It includes four basic steps: deposition, spin-up, spin-off and evaporation, which are shown in Figure 23. In the spin-coating process, a solution is first deposited on the substrate after which the substrate rotated to spread the fluid by centrifugal force. Then, in the spin-off stage, the excess liquid flows to the edge of the substrate. In the final stages, the solution stops flowing as the solvent is gradually evaporated and a thin, homogeneous film is formed. Film thickness and other properties depend on the nature of the solution (viscosity, surface tension, etc.) and on the parameters chosen for the spinning process. Generally, the higher the spin speeds and the longer the spin times, the thinner the films that are formed. In this work Laurell WS-650-23NPPB spin-coater was used. [49]

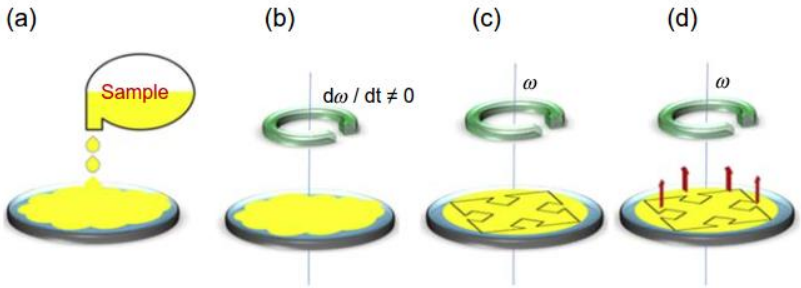

Figure 23. *Steps of the spin-coating process: a) deposition of the solution, b) spin-up, c) spin-off d) evaporation [49].*

Rubbing machine was used to create nanoscopic grooves to the surface of the polymer-coated glass substrate. In this way, liquid-crystal molecules can be oriented in desirable direction, determined by the rubbing direction. The grooves are made using a special rubbing cloth. The substrate is held in its position by vacuum, which is provided by a vacuum pump. In this Thesis, Holmarc HO-IAD-BTR-01 rubbing machine was used.

4.5.3 Transmission electron microscopy

Synthesized gold nanorods were analyzed by transmission electron microscopy. TEM was used to determine the number of particles as well as their size, aspect ratio and size distribution. For TEM imaging, samples are prepared on a copper grid that is coated with a thin layer of carbon.

A TEM works on the same principle as an optical microscope but uses electrons instead of light. Electrons are produced at a cathode and high voltage (100-300 kV) is used to accelerate them. Then the electrons are focused to form a very thin beam (few nm) by electromagnetic lenses. This thin beam goes through the sample and depending on the electron density of the sample, some of the electrons are scattered but others are transmitted through the sample. The specimens viewed in TEM must be thin so that the electrons can interact with the item as they pass through it. TEM does not use a standard lens to produce magnifications; instead, electron beam is passed through a magnetic field, which acts as a lens and produces magnification. Finally, the transmitted electrons hit a fluorescent screen which gives rise to a shadow image. This shadow image can be photographed with a CCD camera to get high-resolution image. The resolution of a basic optical microscope is limited by the wavelength of light (scale of hundreds of nanometers). However, because TEM uses electrons that are accelerated with the voltage of about 100 kV meaning their de Broglie wavelength is on scale of picometers, it is possible to get a resolution a thousand times better than with a light microscope. Because of this, objects on the order of a few angstroms can be seen with a state-of-the-art TEM. In this work, AEM Jeol JEM 2010 transmission electron microscope was used. [50]

4.5.4 UV-Vis-NIR spectroscopy

One of the most useful techniques used in this Thesis work is Ultraviolet-Visible-Near Infrared absorption spectroscopy. UV-Vis-NIR spectroscopy is a common analytical method, and it is based on the fact that some of the molecules, or parts of the molecules, in a solution absorb light differently at different wavelengths.

In this Thesis, a double-beam UV-Vis-NIR spectrophotometer was used. In a double beam spectrometer, light is split into two parallel beams, each of which passes through a cuvette. One cuvette contains the sample dissolved in a solvent and the other cuvette contains the solvent alone. A detector measures the intensity of the light transmitted through the solvent alone (I_o) and compares it to the intensity of light transmitted through the sample (I). The absorbance, A, is then calculated from equation

$$A = -\log_{10}\frac{I}{I_0} \tag{4}$$

The spectrometer scans through all the wavelengths over a selected range. Results are usually presented on a computer screen schematically. This schematic representation is

called an absorption spectrum. The Lambert-Beer law (equation 2) states that the absorbance of a solution is directly proportional to the concentration of the absorbing moieties. Therefore, UV-Vis-NIR spectroscopy can be used to determine the concentration of molecules in a solution. [51]

UV-Vis spectrometer can also be used with different polarizations of light. For example, linear polarizer can be used to study molecular orientation of anisotropic samples. In this case, spectra with the polarization direction of the incident light parallel and perpendicular to the anisotropically aligned molecules are measured and the absorbance for the two perpendicular polarizations are compared. For liquid-crystal samples, the order parameter can be determined with the following equation [31]:

$$S_{exp} = \frac{A_{\parallel} - A_{\perp}}{A_{\parallel} + 2A_{\perp}}, \tag{5}$$

where $A_{\parallel}$ is the absorbance of the light-active moieties in the anisotropic sample orientated parallel to the incident polarized light and $A_{\perp}$ is absorbance with perpendicular polarized light.

In this work, liquid sample spectra were acquired using a Shimadzu UV-1800 UV/vis spectrometer with 1.0 cm plastic or glass cuvettes. Milli-Q water was used as the reference when measured GNR water solution, and chloroform was used when the phase transferred GNR solutions were measured. Polarized UV-Vis spectra of the solid LCE films were measured with Agilent technologies: Cary 60 UV-Vis equipped with Glan-Taylor polarizers unless otherwise stated.

4.5.5 Polarized optical microscopy

Polarized optical microscopy (POM) is a contrast-enhancing optical microscopy technique in which a sample is illuminated with polarized light [52]. This technique is effective for studying materials, for example LC and LCE samples, that have properties which are optically anisotropic and change the polarization of the incident light [53]. In POM a polarizer is used to produce linearly polarized light. A polarizer is an optical component that lets only light with electric field oriented in a specific direction get through. The polarizer can be manually rotated to choose the input polarization of the light incident on the sample. In addition to the first polarizer, there is also a second polarizer as well, often times called the analyzer [52]. In POM, the first polarizer is placed in front of the sample and analyzer is placed after the sample, before the eyepiece and the camera.

The working principle of the POM is simple. Firstly, the polarizer and analyzer are turned so that there is a 90-degree angle between them and therefore no light is passed through. After that, the anisotropic sample is placed on the optical path between the polarizers. Plane-polarized light goes through the sample. because of the birefringence in an anisotropic sample, polarization of light is modulated when travelling in the sample. Now part

of the light can get through the analyzer and an image is formed. The image can be adjusted by rotating the sample. Because the components of an anisotropic sample are aligned at different angles, rotation will cause different parts to be black at different times. This phenomenon occurs because a birefringent sample modifies the polarization of the light only when its optical axes are not on the direction of the original polarization or perpendicular to it. However, if the sample is isotropic, the image remains dark with any orientation of the sample because no light can get through the polarizers. [52]

Importantly, in the case of LCs or LCEs, polarized optical microscopy can be used to detect the existence of the liquid crystal phase and at what temperature they exist [53]. When phase transition of the LCE occurs in certain temperature, the molecular orientation is changed, which can be seen using POM. When an LC is in the isotropic phase, there is no molecular order and the image is black. When temperature decreases, nematic phase with anisotropic molecular orientation appears. Then polarized light gets through and an image is seen. Smectic and crystal phases have different kinds of molecular orientations and therefore the images are also different than nematic phase. Difference between POM images of nematic and smectic phases is illustrated in Figure 24. The technique is effective and relatively inexpensive but it requires that the microscope is connected to a heating plate which allows light to pass through [53]. In this thesis Zeiss Axio Scope.A1 polarized light microscope is used with a hot plate from Linkam Scientific.

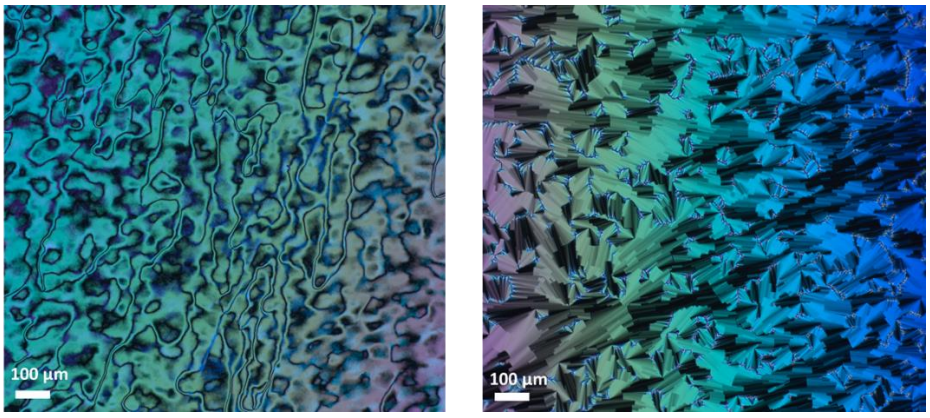

Figure 24. *POM images of 4-pentyl-4'-cyanobiphenyl (5CB) showing nematic phase (left) and 4-octyl-4'-cyanobiphenyl (8CB) showing smectic A phase (right).*

4.5.6 Actuation studies of the LCE films

For photoactuation studies, properly cut LCE films (15 mm x 1 mm; cut along the LCE alignment direction) were taped from one end to the stand. Photoinduced actuation of the films was induced by irradiation with light from LED (Prior Lumen 1600-LED, containing 16 different excitation colors) at room temperature. The actuation behavior was monitored with a camera (Canon EOS 5D Mark III) equipped with 24-105 mm f/4 objective.

Cross-linked UV active azobenzene films were actuated with a wavelength of 365 nm using an intensity of approximately 160 mW cm^{-2}, and the reverse actuation back to the initial state was induced with a 460 nm LED (approx. 310 mW cm^{-2}). Disperse Red 1-containing films were actuated with wavelength of 470 nm and intensity of about 310 mW cm^{-2} whereas the back relaxation occurred thermally.

5. RESULTS AND DISCUSSION

This chapter introduces the results of the measurements and their analysis. These include UV-Vis-NIR spectra, TEM and POM images as well as photographs taken in actuation studies. First, results obtained from synthesizing gold nanorods are presented, followed by functionalization studies. In this work, dissolving GNRs into the liquid crystal elastomer matrix was unsuccessful. Because of poor solubility, GNR-containing LCE films were not fabricated. Therefore, alignment and actuation studies were made on films based on the azobenzene cross-linker and the Disperse Red 1 dye.

5.1 Synthesis of gold nanorods

In this section, results of the GNRs synthesis are presented. Figure 25 shows UV-Vis-NIR spectrum and TEM image of the typical synthesis results obtained when 5-bromosalisylic acid was used as an additive. When longitudinal SPR band maximum is 772 nm, color of the GNR solution is red-brown. Based on Figure 2, this corresponds to an aspect ratio of 3.55 [8]. Based on TEM-images, the average length of rods is 52 nm, width 15 nm, and aspect ratio 3.51. Therefore, the aspect ratio calculated from TEM images matches well with the expectations of linear relationship between longitunal SPR band maximum and aspect ratio.

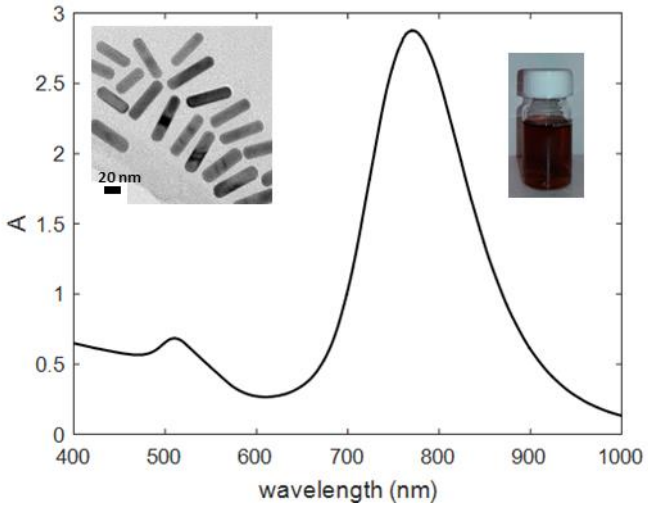

Figure 25. *UV-Vis-NIR spectrum, TEM image and photo of the aqueous GNR solutions synthesized with 5-bromosalisylic acid.*

5.1.1 Synthesis of the seed

Stability of the seed solution was monitored as a function of time with UV-Vis-NIR spectroscopy. As can be seen in Figure 26, during the first two hours there is no significant change in the seed solution. Between 2 hours and 24 hours, the absorbance of the seed solution is reduced but the shape of the spectrum remains the same. The step of the spectra near 350 nm indicates the presence of small seed particles, with diameter of about 5-7 nm. After 30 hours, the absorbance at 540 nm starts to increase, indicating that the seed particles have grown larger, and are thus likely to compromise the quality of the final product [15]. The increasing size of the seeds is evidenced by the spectrum but also apparent from the color of the solution. When the seeds grow larger, the color of the solution changes from dark brown to a bright pinkish red. As Figure 26 illustrates, **the seed particles can be stored for at least two hours**. However, before the seeds can be used it is important to make sure that the remaining reductant is completely decomposed. That is why seed solutions should not be used until after one hour of the addition of the reductant.

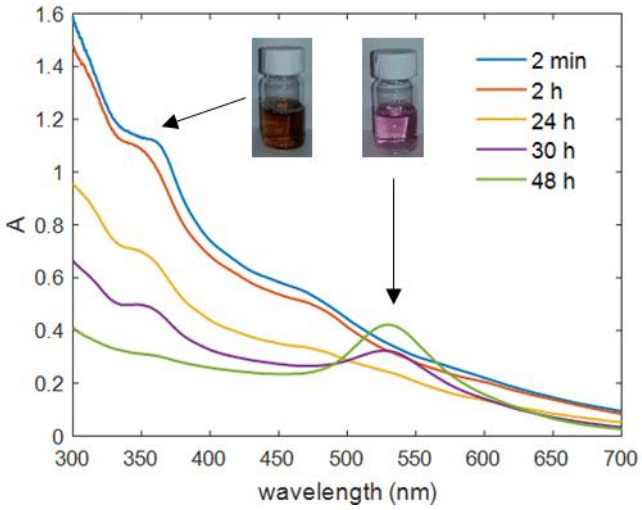

Figure 26. *Monitoring of the development of the seed solution over time.*

5.1.2 Gold nanorod synthesis with and without additive

Gold nanorods were synthesized with 5-bromosalisylic acid, which enhances the micelle behavior of CTAB and therefore improves the shape and size dispersion of the rods. For comparison, the synthesis was also carried out without the additive. Figure 27 shows the spectra of the purified aqueous GNR solutions as well as the TEM images of the nanorods. Bigger TEM images are given in Appendices 1 and 2. The longitudinal SPR maximum wavelength of the two different solutions is not the same but both are still in the infrared region.

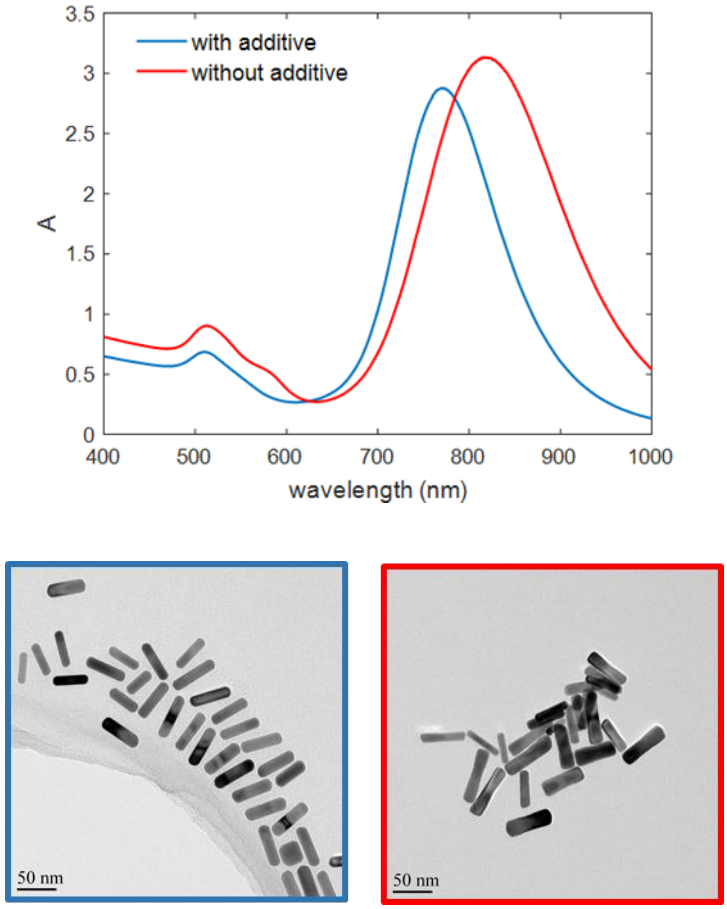

Figure 27. *UV-Vis-NIR spectra of GNR solutions with and without additive (top) and TEM images of the same nanorods (down).*

Aspect ratios of both GNR solutions were calculated from the TEM images by determining the length and width of twenty rods and averaging. Only particles that were truly rod-shaped were accounted for, leaving impurities, like spherical particles, out of calculations. The results are given in Table 4. The aspect ratio of the additive-containing GNRs is lower than the GNRs without additive, which correlates with the value of the longitudinal SPR peak maximum wavelength: lower AR means lower longitudinal SPR maximum wavelength value. Average width of the rods is the same.

Table 4. *Longitudinal SPR maximum wavelength ($\lambda_{LSPR,max}$), average length of the rods (l), average width of the rods (w) and aspect ratio (AR) and standard deviations.*

GNR solutions	$\lambda_{LSPR,max}$ (nm)	*l* (nm)	*w* (nm)	AR
With additive	772	52 ± 5	15 ± 2	3.51 ± 0.39
Without additive	822	61 ± 10	15 ± 4	4.16 ± 0.87

Size dispersion of the GNR solutions can be estimated in many ways. First, standard deviation of the AR of the rods synthesized without the additive is over two times as big as that of the rods synthesized in the presence of the additive. Secondly, FWHM values of the longitudinal SPR peaks can be compared. When the additive is used, FWHM is 45 nm lower (123 nm) than when the additive is not used (168 nm), as can be clearly seen in Figure 27. The presence of by-products can be seen from the TEM images as well as from the shoulder of the transverse SPR peak in the UV-Vis-NIR spectra. The TEM images (see Appendices 1 and 2) show that that there are more spherical and square-shaped particles in the additiveless GNR solutions. The shoulder is clearly present in the UV-Vis-NIR spectrum at the wavelength of about 580 nm (Figure 27, red curve), whereas it is absent in the synthesis product obtained with the additive. The morphology of the GNRs can be illustrated with high-magnification TEM images, which are given in Figure 28. The images indicate that the surface of the rods synthesized without the additive is more rough than for the ones synthesized with the additive. These parameters indicate that **when the additive is used in the synthesis of the GNR, the size dispersion of the particles is smaller and the morphology is better-defined.**

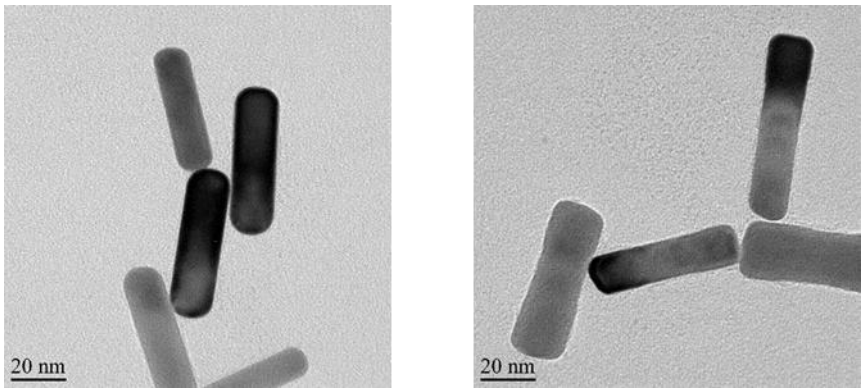

Figure 28. *High magnification TEM images of the rods synthetized using the additive (left) and without using the additive (right).*

Concentrations of the GNR solutions were calculated as inroduced in Section 2.7. The molar extinction coefficients are determined from the data provided by Murphy *et al*. [13]. Both concentrations and extinction coefficients are presented in Table 5. The width of the cuvette used was 1.0 cm. It is noteworthy that even though absorbance in the additive GNR solution is smaller than in the non-additive solution, its GNR concentration is still higher. Absorbance of the solution depends both on the concentration and the molar extinction coefficient as equation 2 states. The molar extinction coefficient depends on the aspect ratio of the rods. As can been in Figure 8, the extinction coefficient of the rods gets smaller when the aspect ratio is lowered. Because the aspect ratio of the additive GNR solution is lower, its extinction coefficient is also lower. This is why the concentration is higher even though the absorbance is lower.

Table 5. *Maximum absorbance of the longitudinal SPR peak ($A_{LSPR,max}$), extinction coefficient (ε), and calculated concentration (c) of the nanorod solutions.*

Solutions	$A_{LSPR,max}$	ε (cm^2 per rod)	c (rods ml^{-1})
With additive	2.88	$7.42 \cdot 10^{-12}$	$3.9 \cdot 10^{11}$
Without additive	3.13	$8.45 \cdot 10^{-12}$	$3.7 \cdot 10^{11}$

5.1.3 Stability of the aqueous gold nanorod solutions

UV-Vis-NIR spectroscopy can be used to monitor the stability of the GNR solutions because aggregation of the rods changes their optical properties. When aggregation occurs, SPR modes of the rods change, because the conduction electrons of the rods become delocalized and they are shared amongst neighboring rods. When this occurs, the SPR shifts to lower energies, causing the absorption peaks to broaden and to red-shift to longer wavelengths. Moreover, the original absorption peaks will decrease in intensity because of the decrease in the number of stable rods. [54]

Figure 29 shows the spectra of the GNR solutions measured immediately after centrifugation and five weeks afterwards. Because there is no significant change in the shape of the spectra or in the absorbance, both solutions (with or without the additive) are concluded to be stable at least for a time period of five weeks.

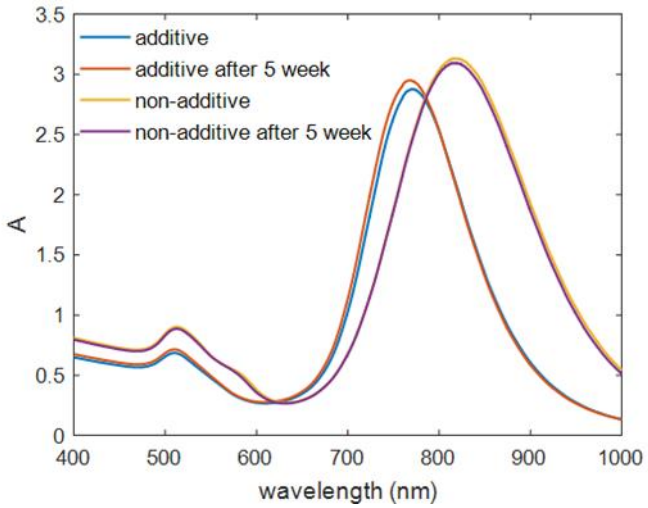

Figure 29. *Stability of the GNRs in water over a five week period with and without additive.*

5.1.4 Centrifugation of the gold nanorod solutions

Figure 30 presents the spectra of **the additive GNR solutions** before and after two centrifugation steps. The spectrum of supernatant is also measured.

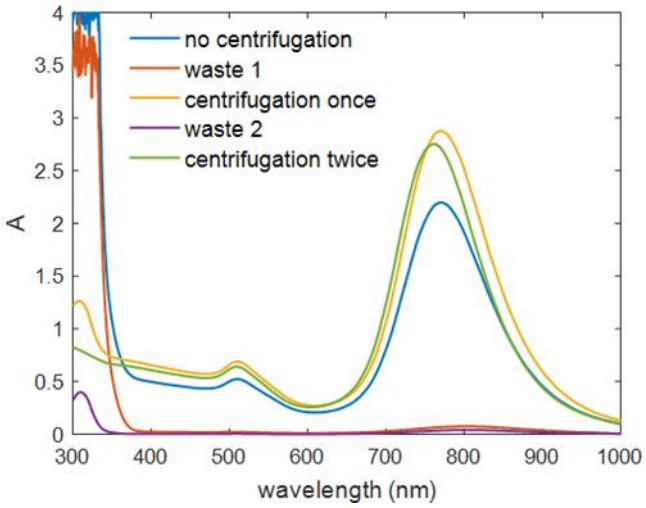

Figure 30. *Spectra of the washing process of the GNR solutions. In first centrifugation cycle absorbance is increased, because solution was concentrated.*

Table 6 indicates how $\lambda_{LSPR,max}$ and FWHM change during the washing process. After the first centrifugation cycle, neither the longitudinal SPR peak maximum nor the FWHM change, which indicates that there is no significant change in the aspect ratio of the rods. However, after the second centrifugation step, small blue-shift occurs and FWHM of the rods reduces by 4 nm. This indicates that the size dispersion of the nanorods is slightly improved.

Table 6. *Longitudinal SPR maximum wavelength and full width half maximum before and after each centrifugation.*

Centrifugation	$\lambda_{LSPR,max}$ (nm)	FWHM (nm)
No	772	123
Once	771	123
Twice	761	119

From the spectra in Figure 30 one can also evaluate how well the purification process works. Firstly, there are no significant peaks in the spectra of the supernatant at the wavelength range of longitudinal and transverse SPR modes. This indicates that supernatant does not contain rods. Secondly, the high absorption at wavelength below 400 nm comes from 5-bromosalisylic acid. After the first centrifugation step almost all 5-bromosalisylic

acid is removed and after the second centrifugation step it is removed completely. Overall, **centrifugation is a very powerful tool in the cleaning process**.

The centrifugation also plays an important role in the stability of the GNRs. When the rod solution is not centrifuged at all, blue-shift was observed during one week. This is due to the overgrowth of the rods where unreacted starting materials are reducing on the surface of the rods. The reduction probably occurs on the side of the rods, which is why the width increases and the aspect ratio decreases, which is seen as a blueshift of the spectra [8].

5.1.5 Tuning the aspect ratio

In this work, the aspect ratio and the wavelength of the longitudinal SPR peak were adjusted by changing the amount of silver nitrate in the growth solution. When more silver nitrate was added, the position of the longitudinal SPR absorption maximum was shifted to longer wavelengths. Figure 31a presents the spectra of the solutions (synthesized with the additive) with different amounts of silver nitrate. In Figure 31b, the wavelengths of maximum absorption are shown as a function of silver nitrate concentration. As can be seen, this dependence is linear within concentration range of 50-90 μM. The absorption wavelength grows with increasing silver nitrate concentration because rods are longer and they absorb more light. Silver nitrate concentration was calculated using the final volume of growth solutions and the known concentration and volume of the added silver nitrate solution. The aspect ratio tuning is confirmed by TEM images, which are also given in Figure 31c-e.

It is worth noting that **Figure 31b is only for illustrative purposes**. The synthesis is very sensitive to a variety of different factors, such as the concentration of the stock solutions, acidity of the Milli-Q water, and even the shape of the reaction vessels. Therefore, when the synthesis is done in a different laboratory, results may differ from the ones presented here. Because of that, synthesis should be first done in small volumes (10-20 ml) to find out the real relationship between longitudinal SPR wavelength and concentration of silver nitrate. This experiment was carried out with the scale of 20 ml.

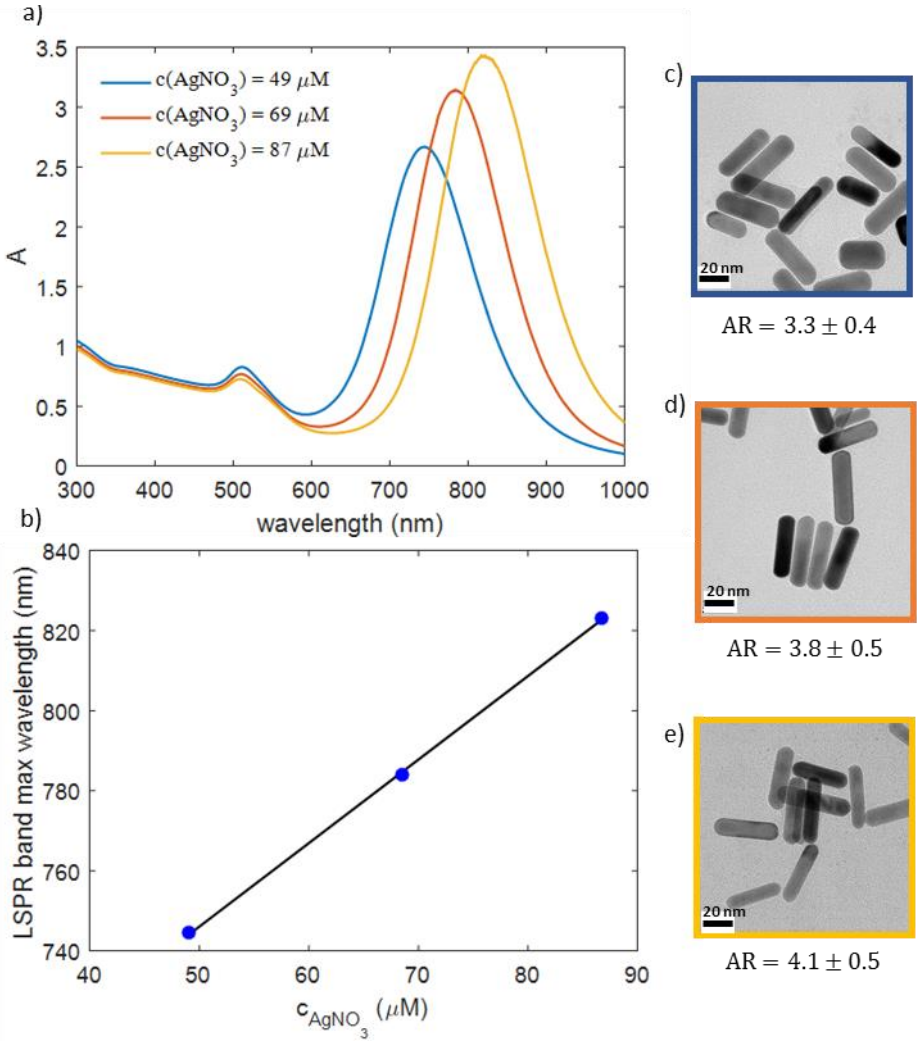

Figure 31. *a) Spectrum of the growth solutions (with additive) with different silver concentrations, b) a relationship between longitudinal SPR peak maximum and silver concentration of the solutions and linear fit the data, and c-e) corresponding TEM images.*

5.2 Functionalization of gold nanorods

Two attempts were made to functionalize GNRs. First, dodecanethiol (Figure 9) was used, but the phase transition did not occur properly. However, GNRs were transferred to organic phase using a two-step procedure where the rods were first pre-stabilized with thiolated polyethylene glycol (Figure 9). In the next two sections the functionalization procedures are discussed in more detail. UV-Vis-NIR spectra and TEM images of the organic GNR solutions are shown in cases where the phase transfer was successful. Concentration of the new ligands was optimized to obtain the best functionalization. The functionalization was only carried out for the GNR solutions synthesized with the 5-bromosalisylic acid as an additive.

5.2.1 Phase transfer with dodecanethiol

In this method, the phase transfer of the GNRs occurs in two steps. First, the GNR solution is mixed with the new ligand, dodecanethiol. After the addition of the DDT to the GNR solutions, the two-phase solution was shaken vigorously. However, if shaking was too hard, foam was created. Foaming may make it difficult for the new ligand to attach to the surface of the GNR. Therefore, the shaking should not be too vigorous.

In the second step, acetone and toluene were added to the solution, which resulted in a colorless organic phase on top and reddish water phase on bottom. When more acetone was added, GNRs visibly rose from the water phase to the organic phase. At the interface between the two phases, some aggregated particles were seen by naked eyes. When the organic phase was decanted off, care was taken that none of the aggregated particles were decanted. This procedure was repeated about five times until the water phase was colorless. The organic phase now contained both toluene and acetone. To remove the acetone, the solution was placed in a rotavaporator. Because the boiling point of acetone is lower than that of toluene, acetone was evaporated first. When acetone was evaporated, the solutions lost their reddish color and visible aggregates were observed on the wall of the vessel, and the remaining toluene solution was colorless. The UV-Vis-NIR spectrum of the toluene solution was measured but there were no signs of the longitudinal or transverse SPR bands of the rods.

The above result indicates that the phase transfer was not successful. Different shaking times (1 h - 1 day) and different amounts of DDT were tried on order to get better functionalization. However, the end result was always the same: the rods were transferred to the mixture of toluene and acetone, but when acetone was evaporated off, the rods aggregated.

One of the reasons why the phase transfer was not successful may be that the new ligand, DDT, cannot displace CTAB molecules on the surface of the GNRs. When DDT is mixed with GNR solutions, some of the DDT molecules should adhere onto the surface of the GNRs. If, however, some of the rods are not in contact with DDT, these rods aggregate in the second step. Another reason may be related to kinetics. When acetone is added, it removes CTAB from the surface of the rods [25]. If binding kinetics of the DDT to the surface of the GNR is not fast enough, aggregation occurs. These reasons explain why aggregated particles were seen between water and organic toluene phase and why the aggregation of the GNRs occurs when acetone is evaporated.

5.2.2 Phase transfer with mPEG-SH and DDT

Because the functionalization of the GNRs with DDT was not successful, another procedure was tried. GNRs were **pre-coated** with a small amount of thiolated polyethylene glycol (average molar mass 6000 g mol^{-1}) to avoid aggregation. After pre-stabilization

dodecanethiol was added in excess to fully coat the GNRs and to make them hydrophobic and soluble in the organic phase. Figure 32 shows the spectra of the initial aqueous GNR solutions where the rods are coated with CTAB (blue curve), aqueous solutions of the mPEG-SH-coated rods (red curve), and chloroform solutions of the DDT-coated rods (yellow curve). The amount of solvent is the same in all solutions so that the absorbance of the longitudinal SPR peaks can be compared. TEM-images from the final, organic GNR solutions are given in Figure 32 as well.

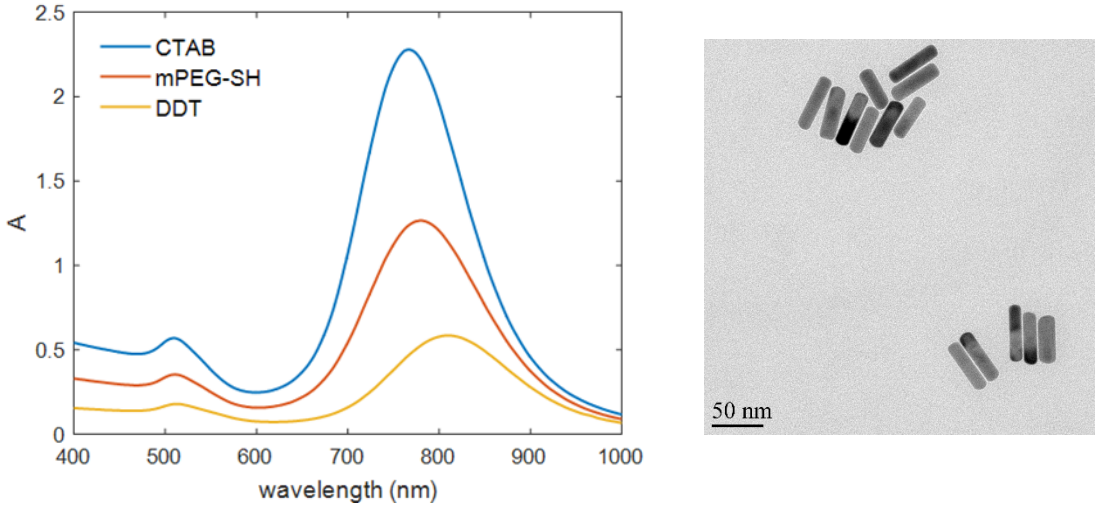

Figure 32. *Spectrum of the GNR solutions coated with CTAB, mPEG-SH and DDT (left) and TEM images of the DDT coated GNRs.*

At first, aqueous mPEG-SH solution was combined with the GNR solution, and after 2 h of shaking, the UV-Vis-NIR spectrum of the solution was measured. Because the longitudinal and transverse SPR peaks are clearly visible, pre-functionalization was successful. However, absorbance of the longitudinal SPR peak was decreased almost by a half. The wavelength of the longitudinal SPR peak was also red-shifted from 767 to 780 nm. After the addition of the DDT and chloroform, phase transition occurred upon vigorous stirring. The absorbance of the longitudinal SPR peak is further reduced by a half and the longitudinal plasmon band red-shifts from 780 to 811 nm.

Because the absorbance of the longitudinal SPR peak is reduced, some GNRs are lost during functionalization. In the pre-stabilization step some of the rods may have aggregated. During the actual phase transition, some of the rods may still remained in the aqueous phase because of the improper DDT coating.

The aspect ratio of the original GNRs was 3.66 ± 0.56 and after the phase transfer 3.67 ± 0.49. Because the aspect ratio of the rods remained the same upon the phase-transfer process, the red-shift of the longitudinal SPR peak cannot be explained by the change of AR. It is more likely that the red-shift occurs because of the change in refractive index (1.33 for water and 1.44 for chloroform [55]) of the solvent. During pre-functionalization, the red-shift is due to the different ligand on the surface of the GNRs. The red-

shift of the longitudinal band during the phase-transition process is in line with other studies [16; 17; 19]. Table 7 summarizes the values of longitudinal SPR maximum wavelength and the absorbance as well as values of FWHM and aspect ratios. According to FWHM values, the longitudinal SPR peak is broadening when phase transition occurs. This may be due to small extent of aggregation of the particles. However, the rods are well separated from each other in the TEM images, which confirms the absence of large-scale aggregation.

Table 7. *Longitudinal SPR peak maximum's wavelength, absorbance, full width half maximum of the peak and aspect ratio of the rods.*

Solutions	$\lambda_{LSPR,max}$ (nm)	$A_{LSPR,max}$	FWHM (nm)	AR
CTAB	767	2.28	129	3.66 ± 0.56
mPEG-SH	780	1.27	141	-
DDT	811	0.59	148	3.67 ± 0.49

Proper amount of mPEG-SH was monitored to achieve the highest absorbance in the phase-transferred GNR solutions. Figure 33 shows that the best result was achieved when 4 mg of mPEG-SH per 1 ml of GNR solution was added. If less mPEG-SH was used, the absorbance was reduced. This may be because there are not enough of mPEG-SH-molecules to bind to the surface of the GNRs [21]. If less than 2 mg ml^{-1} of mPEG-SH is used, pre-functionalization fails and the rods aggregate. However, if more than 4 mg ml^{-1} of mPEG-SH is used, the absorbance was smaller again. When too much mPEG-SH is added, it can prevent DDT from attaching onto the surface of the nanorods and aggregation occurs after the second step [21].

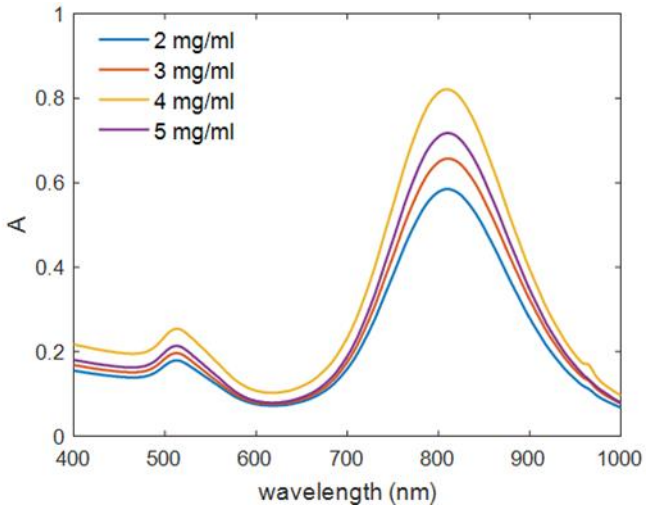

Figure 33. *Spectra of the phase-transferred GNR solutions with different amounts of mPEG-SH in the pre-stabilization step.*

5.3 Mixing gold nanorods and LCE molecules

Liquid crystal monomer (400 mg) and cross-linker (150 mg) (see Figure 22) were dissolved in chloroform (3 ml). The LCE molecules dissolved well and no heating was needed. GNRs-LCE solution was made by adding 5 mg of initiator and a different amount of phase transferred the GNR solution to the LCE solution. Figure 34 presents UV-Vis-NIR spectra of the phase transferred gold nanorod solutions (blue curve) and LCE solutions (mentioned above) which contain 1.2 ml GNR solutions (red curve). FWHM of the longitudinal SPR peak is increased only by 5 nm. This indicates, together with the shape of the spectrum, that **the GNRs retain their plasmonic properties in the LCE-chloroform solutions.**

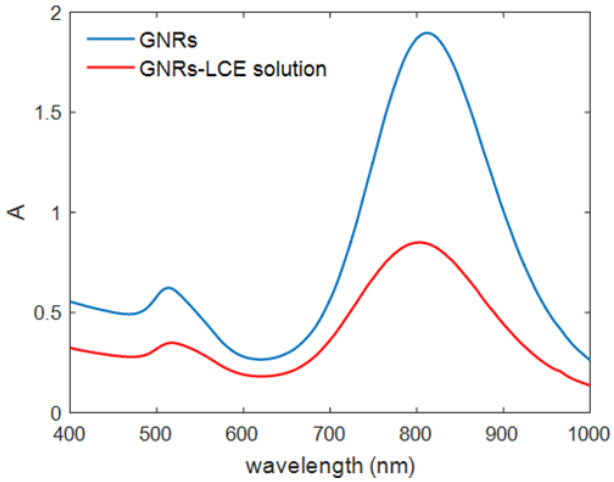

Figure 34. *UV-Vis spectrum of phase transferred GNR solutions and GNR-LCE solution in chloroform.*

However, when the solvent was evaporated at 90 ℃, the rods aggregated, which was noticed from the disappearing red color of the solutions. After photopolymerization, UV-Vis-NIR spectrum of the film was measured. This spectrum had no longitudinal or transverse SPR absorptions peaks, which indicates that the GNRs are insoluble with the liquid crystal monomer and cross-linker used. Many attempts were made to improve the solubility of the GNRs, including sonication and adding different amounts of GNRs to the solution and different evaporating temperatures, but same solubility results were obtained.

There are a few reasons why aggregation of GNR may occur when attempts are made to dissolve rods with LCE molecules. Firstly, the aggregation of GNRs takes place because of the poor solubility of the DDT-coated rods with the LCE molecules. Both LCE molecules are soluble in chloroform but evaporation of the solvent leads to insolubility because DDT cannot prevent core−core attractions between the rods well enough. Secondly, the aggregation takes place because the GNRs disturb the LC director, which results in elastic interparticle forces and ensue aggregation. Thirdly, functionalization may not be complete which leads to aggregation.

5.4 Characterization of fabricated LCE films

Two LCE solutions were made, containing the monomer, cross-linker and initiator listed in Figure 22, together with UV-absorbing azobenzene and Disperse Red 1. The used UV-absorbing azobenzene can be classified as an azobenzene-type molecule while Disperse Red 1 is of pseudostilbene-type. From each LCE solution, two films were photopolymerized: one with planar and one with splay alignment (see Figure 17). Therefore, a total of four LCE films were fabricated and characterized in this work.

Firstly, nematic-to-isotropic and solid-to-nematic phase-transition temperatures of the two LCE mixtures were characterized with POM. For UV-LCE sample these temperatures were about 60 ℃ and 30 ℃, respectively. For Vis-LCE nematic-to-isotropic phase transition temperature was 60.5 ℃ whereas the nematic phase still occurs still even at the room temperature. Photopolymerization has to be carried out at the temperature where the mixture is in the liquid-crystalline phase [22]. Based on this analysis, both samples were polymerized at 50 ℃.

5.4.1 Alignment studies of the planar LCE films

After polymerization, the planar sample cells were investigated with POM and polarized UV-Vis spectroscopy. POM images were taken so that the polarization of input light was parallel to the rubbing directions (0° angles between the polarizer and the rubbing direction) and so that the angle between rubbing direction and light polarization was 45° as shown in Figure 35. POM pictures taken at 0° angle are darker because the LCE molecules, which are now arranged in the direction of polarization of the light, do not modify the polarization of the input light. In the case of perfect alignment, the picture would be completely dark. The samples exhibit brighter images between crossed polarizers when the director axis is set to 45° angle because the samples now modify the polarization of the input light more effectively. Evenly bright pictures indicate homogeneous mesogen alignment in the sample. However, because the brightness difference between the pictures taken with 0° and 45° angle is not very large, there is some disorder in the molecular alignment. Moreover, because there are dark and light areas on the same image, samples may be somewhat phase separated.

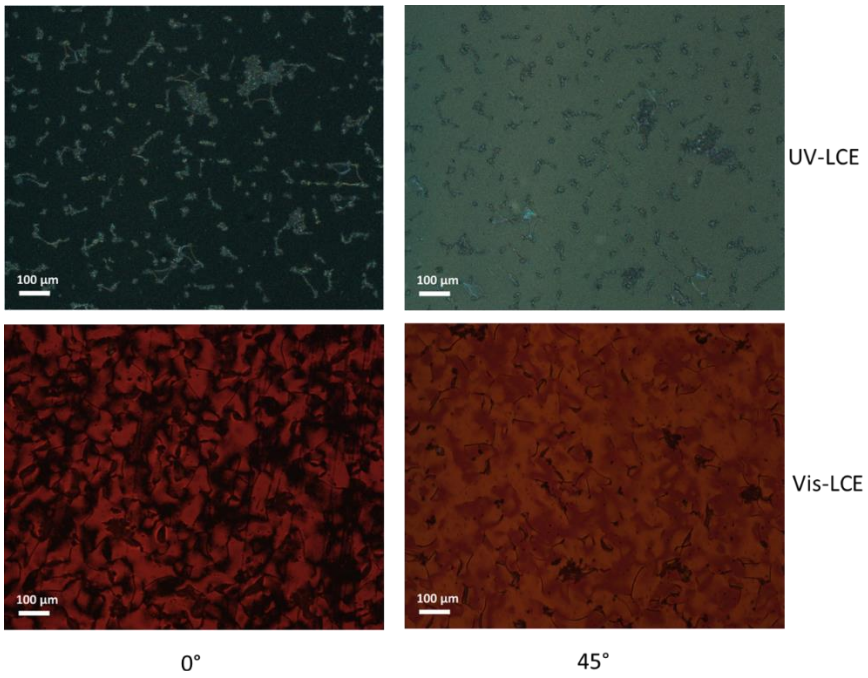

Figure 35. *Polarized optical micrographs for UV-LCE (top) and Vis-LCE (bottom), taken at 0° (left) and 45° (right) angles between the polarizer and the rubbing direction.*

Figure 36 presents unpolarized UV-Vis spectra of both planar sample films. Because the fabricated films were thick (30 µm) and the azobenzene concentration was relatively high (5 mol-%), they absorb light very strongly. The sensitivity of the detector of the spectrometer was not good enough to accurately detect such large absorption, and for that reason, the absorption maxima are not shown properly. To get better spectra, thinner films or lower azobenzene concentration should be used. However, the spectra given in Figure 36 give a rough estimate on the absorption peak maximum; *ca.* 360 nm for the UV-LCE and 500 nm for the Vis-LCE. Moreover, Figure 36 shows that these two samples behave differently at NIR wavelengths. For the Vis-LCE sample, the absorbance at > 650 nm, where no light absorption is expected, is low (~0.1) and flat. However, for the UV-LCE, the measured absorbance at long wavelengths is about 0.5 and increases with decreasing wavelength. Because none of the sample components absorbs above 600 nm, it scatters light strongly. This indicates that photopolymerization process did not succeed as well as in the Vis-LCE sample. This may be due to different polymerization wavelengths (420 for UV-LCE and 375 nm for Vis-LCE) used for the activation of the initiator (Irgacure 819). Irgacure 819 has the absorption maxima at 295 nm and 370 nm [19]. Therefore, the initiator was perhaps poorly activated and polymerization was not complete. In the future, other photoinitiators could be considered. On the other hand, the starting materials are perhaps not mixed with each other completely. If all starting materials would have been dissolved in the solvent, proper mixing could have been guaranteed.

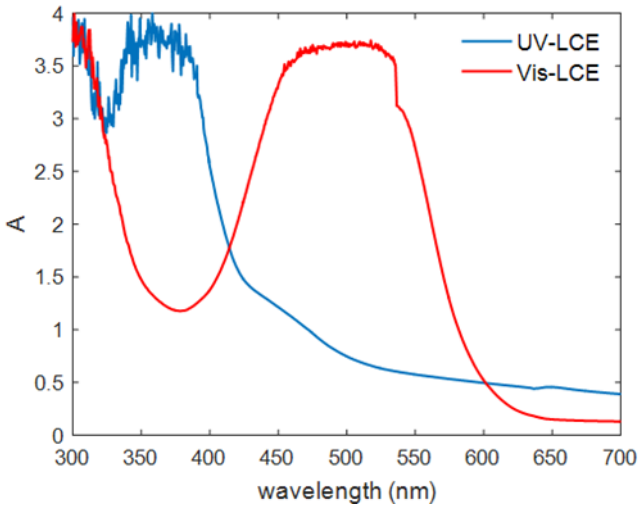

Figure 36. *Unpolarized UV-Vis spectra of the polymerized films taken from Shimadzu UV-1800 UV-Vis spectrometer.*

Figure 37 presents the polarized UV-Vis spectra of the planar films. The spectra were taken so that the polarization of light was parallel and perpendicular to the rubbing direction. The absorbance has been corrected to zero at 750 nm wavelength so that scattering of the films does not interfere with the determination of the order parameter. **The order parameter of the samples** was determined as follows: the value of the corrected absorbance was read from the parallel and perpendicular UV-Vis spectra at the same wavelength, and the order parameters were calculated using equation 5. Averaging of twenty values was performed over wavelength ranges, which are as close as possible to the maximum absorbance but not in the noise area. Order parameter for UV-LCE film was determined from n $\rightarrow \pi*$ transition of azobenzene and from $\pi \rightarrow \pi*$ transitions for Vis-LCE. The results are given in Table 8.

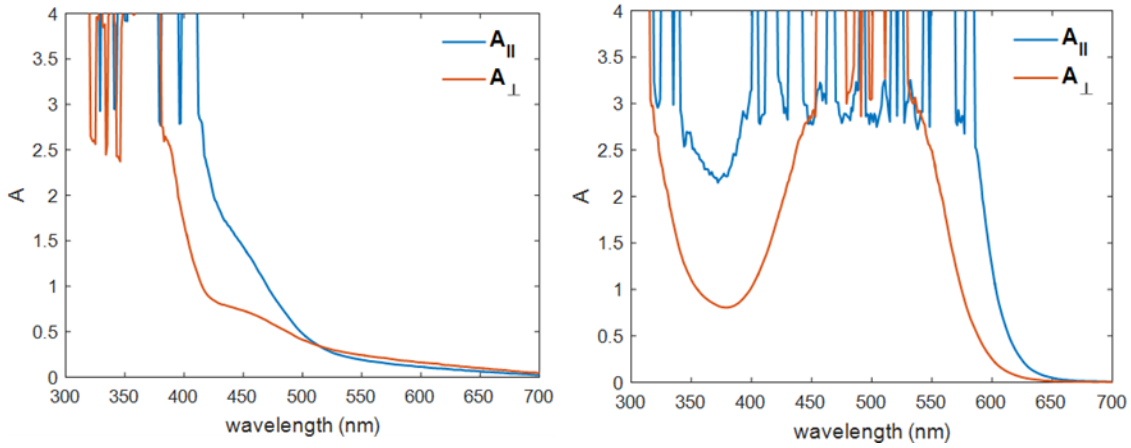

Figure 37. *Polarized UV-Vis spectra for UV-LCE (left) and Vis-LCE (right) taken with Cary 60 UV-Vis spectrometer. $A_{\parallel}$ and $A_{\perp}$ correspond to absorption parallel and perpendicular to the rubbing direction, respectively.*

The UV-active azobenzene is a cross-linker and it is a part of the LCE network. Therefore, experimental order parameter indicates not only the orientation of the dye but also orientational order of the whole LCE matrix. DR1, on the other hand, is not a part of the LCE network and therefore the order parameter indicates orientational order of the DR1. However, because the orientation of the LCE-matrix determines the order of the dye, the order parameter gives an indication of the alignment of the LCE network as well.

Table 8. *Maximum absorbance wavelength of the azobenzene ($\lambda_{\mathrm{max,azo}}$), wavelength interval where the order parameter was determined ($\lambda_{interval}$) and the order parameter (S) with standard deviation.*

Sample	$\lambda_{max,azo}$ (nm)	$\lambda_{interval}$ (nm)	S
UV-LCE	360	417-436	0.31 ± 0.03
Vis-LCE	500	590-609	0.56 ± 0.01

As Table 8 shows, the order parameter of the UV-LCE is quite small (0.31), because order parameters as high as 0.75 have been reported for a cross-linked azobenzene matrix [42]. Because the used azobenzene absorbs light at 420 nm (see Figure 20), which was used at photopolymerization, this light may have isomerized azobenzenes and reduced the order of the molecules. Another explanation could be the improper rubbing of the glass cell due to which the LCE molecules are not aligned properly. Moreover, order parameter for UV-LCE film was determined from n $\rightarrow \pi*$ transition of azobenzene, which has notable absorption in the *cis* isomer (See Figure 20). Therefore, if even some of the azobenzene molecules are in *cis*-form due to room light, it reduces the value of the order parameter. However, order parameter for the Vis-LCE sample (0.56) is high. LCE films containing DR1 fabricated with photopolymerization have not been reported. Therefore, comparing the order parameter to other studies is difficult. However, the determined order parameter is similar to those previously obtained in our group.

5.4.2 Actuation studies of polymerized films

Photoinduced bending behavior of the fabricated UV-LCE and Vis-LCE films was investigated. All four films (two planar-aligned and two splay-aligned) showed good actuation, when irradiated with light at appropriate wavelength, *i.e.*, close to the absorption maximum.

Figure 38 shows a series of photographs taken from the actuation of the UV-LCE films. When the films were irradiated with UV light (365 nm), both of them bent. When the UV light was switched off, the films retained their shape. Little relaxation can be observed after the UV light was turned off. The films returned to their original shape when irradiated with visible blue light (460 nm). After the blue light is switched off, little relaxation

can be observed. Noteworthy is that similar bending process was seen when the experiment was repeated in the same film, *i.e.*, the results shown are reproducible. Bending of the planar film takes about 6 s, while bending of splay takes twice as much time. The difference between the bending times is due to curling of the splay film. At the end of the bending process, the splay-aligned film curls which may be due to imperfect alignment of the film.

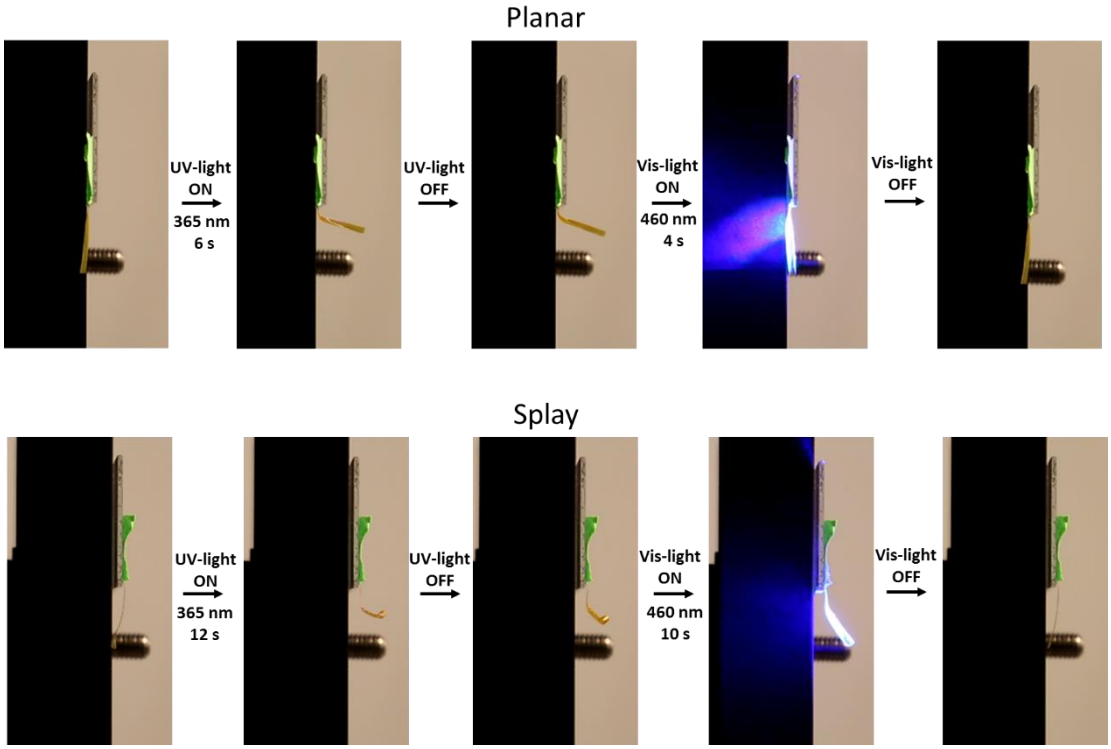

Figure 38. *Photographs of the actuated film, containing UV active azobenzene, with the planar (up) and splay (bottom) orientations.*

The bending mechanism of UV-LCE is mainly based on a photochemical effect. In planar films, bending occurs because of relatively high dye concentration (5 w-%) resulting in high absorption of the film. UV light is strongly absorbed by the film and therefore it cannot penetrate through the whole film thickness, which results in a gradient in the isomerization-induced reduction in the LC order and bending of the film [42]. Before irradiation, mesogens are in the *trans*-form and film has orientational order. After isomerization, mesogens are in the *cis*-form, which causes disorder of the LCE matrix and the film bends. In splay-aligned films, the bending mode is emphasized, because alignment of the two sides of film are not the same. However, from Figure 38 this is difficult to see, because the splay-aligned film is curled. When the splay-orientated films are actuated, homeotropically aligned sides expand and homogeneously aligned contract at the same time and bending occurs. Figure 39 presents schematically how bending of the splay-film occurs. Thermal relaxation times of azobenzene-type molecules are long and therefore the film retains its shape after UV light is turned off. Until after the next light stimulation, the

molecules relax back from the *cis*-form to the *trans*-form and the order of the LCE matrix is restored.

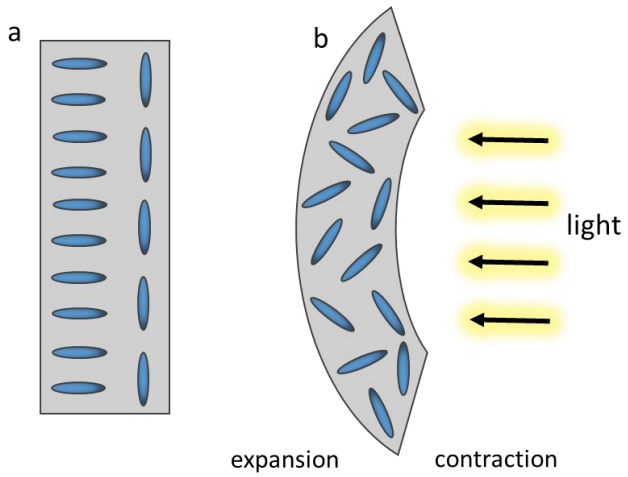

Figure 39. *Splay-aligned film: a) before irradiation mesogens are in order; b) after irradiation mesogens are in disorder because of photochemical or photothermal activation, and homeotropically aligned side expands while the homogeneously-aligned side contracts, causing the bending.*

Figure 40 presents photographs of the Vis-LCE, containing DR1. When visible light (470 nm) is switched on, the films bend in about 2 s. When the light is switched off, the films relax back to their original shapes relatively quickly (in seconds). In photothermal effect, dye molecules absorb light and convert it to heat, which is then transferred to the LCE matrix and bending can occur. Because DR1 is a functionalized azobenzene molecule, it can undergo photoisomerization under visible light. Distinguishing between these two mechanism based on the studies made in this Thesis is quite hard.

In photothermal mechanism, the explanation why splay alignment Vis-LCE film bends is also based on the different alignment of the mesogens on the opposite sides of the film, leading to one side to expanding and the other contracting (see Figure 39). Interestingly, also the planar-aligned film bends. Usually, planar films should not bend significantly if photothermal effect is considered. However, there are a couple of reasons for this behavior. One reason may be a temperature gradient. Because of a high dye concentration and relatively thick film, absorption of the film is high and light does not penetrate through the whole film thickness. As a result, the order change is concentrated at the incident surface instead of the second surface. This leads to bending of the whole film. Other reason could be improper alignment of the LCE molecules in the film. However, the relatively high order parameter ($S > 0.5$) of the planar film does not support this. Finally, photochemical effect cannot be ruled out. Because of the high dye concentration, the effect of the *cis-trans* isomerization may become significant.

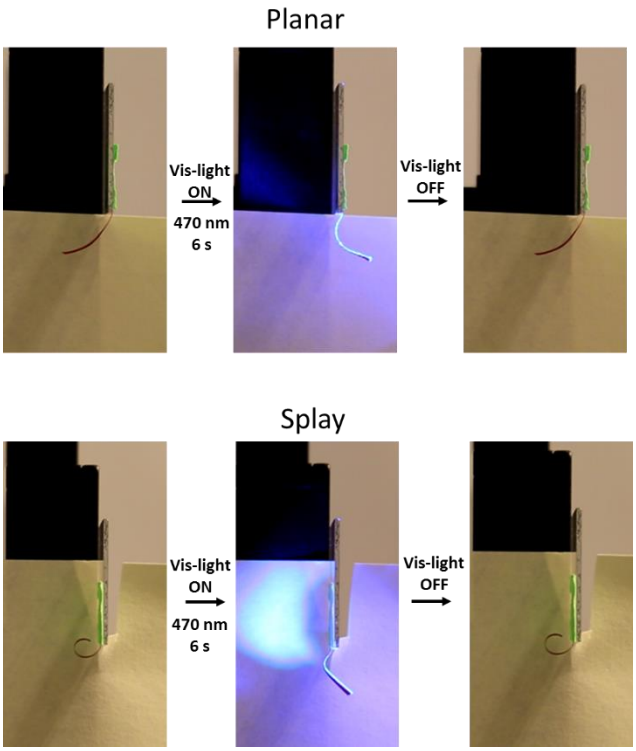

Figure 40. *Photos of the actuated film containing DR1 dye, with the planar (up) and splay (bottom) orientation.*

Quick relaxation of the film can be explained with both photochemical and photothermal mechanisms. In photochemical effect, quick relaxation is due to the short relaxation time of pseudostilbene-type molecules. In photothermal effect, relaxation is fast because of the fast light-to-heat conversion rate of the DR1 dye. When light is turned off, DR1 does not absorb light and it cannot produce any heat which could then heat the LCE matrix, and therefore surrounding air can cool the film quickly.

Large initial curling of the DR1 splay-aligned film can be explained with the difference between polymerization and the actuation temperature if the photothermal effect is considered. Films were polymerized at 50 ℃ and actuated at room temperature (25 ℃). When temperature decreases, the molecular order of the film increases, and therefore homeotropic side of the film tends to contract and the homogenously aligned one to expand at the same time and as a result the film bends. This also explains why the film curls at the opposite direction when it is irradiated. When temperature of the film increases because of photothermal heating, homeotropic side expands and homogenous side contracts and opposite curling is observed. If the initial curl of the splay film is taken into account, it can be concluded that bending behavior of the splay film is stronger than that of the planar film.

6. CONCLUSIONS

The present Thesis work was carried out in 2016 at the Smart Photonics Materials group at Tampere University of Technology. Photoactuable liquid-crystal elastomer materials are a new research topic for the group, initiated only in 2015. Fabrication of the liquid crystal elastomer films has focused on azobenzene-containing actuators, and this was the first attempt by our group to utilize gold nanorods in photoactuation.

In this Thesis work, **the solubility of the gold nanorods and photopolymerizable liquid crystal molecules was studied**, and attempts were made to fabricate liquid-crystal films based on gold nanorods. Special attention was paid to learn to synthesize monodisperse gold nanorods of different size and aspect ratio, and to functionalize them in a proper way. The purpose was to adopt the most precise synthesis and characterization methods, following the latest guidelines published in the literature. Even though photoactuation of the gold-nanorod-doped liquid-crystal elastomer films was unsuccessful, actuation of films containing cross-linked UV-absorbing azobenzenes, and doped visible-absorbing azobenzenes were studied.

Gold nanorods were synthesized with seed-mediated growth method and CTAB was used as a surfactant. The aspect ratio of the gold nanorods was controlled in the range of 3.0-4.1, to yield longitudinal surface plasmon resonance band between 750-830 nm. The aspect ratio of the gold nanorods was tuned by varying the amount of silver nitrate in the growth solutions. The gold nanorods were synthesized with 5-bromosalisylic acid as an additive, which was noticed to improve the size dispersion and morphology of the nanorods significantly compared to the additiveless synthesis. Gold nanorods were functionalized successfully with the combination of poly(ethylene glycol) methyl ether thiol with average molar mass of 6000 g mol^{-1} and dodecanethiol. Functionalization was also tried with only dodecanethiol but this led to aggregation of the rods.

Functionalized gold nanorods were soluble in liquid crystal monomer and cross-linker when all components were dissolved in chloroform. However, aggregation occurred when the solvent was evaporated, suggesting that **future work is needed for obtaining free-standing, gold-nanorod-doped, liquid-crystal elastomer actuators.** It would be especially important to perform further and more comprehensive studies on functionalization of the GNR that have a crucial role when the GNR are doped in liquid-crystal elastomer network. Functionalization studies can be continued with used thiolated polyethylene glycols and dodecanethiol, but supplemental stability studies need to be made. Another solution could be to try other molecules to functionalize gold nanorods, for example, the use of amines may be a viable option. The second solution may be to try different liquid-crystal elastomer monomers and cross-linkers. However, most liquid-crystal elastomer molecules used in the photopolymerization are chemically quite similar thus limiting this

option. On the other hand, thermal polymerization technique based on silicon chemistry could also be worth consideration. Finally, one solution could be to use another surfactant than CTAB when gold nanorods are synthesized. CTAB may bind too strongly to the surface of the nanorods and therefore other molecules cannot replace it. Citrate may be one surfactant that can be considered to replace CTAB.

Two other chromophores, both azobenzene derivatives, showed good solubility into the liquid-crystal elastomer matrix. Both planar and splay-oriented films exhibited photoinduced bending upon irradiation with UV/Visible light. In particular, efficient bending of the planar Dispersed Red 1-containing film should be studied more extensively. However, quantification whether the photoactuation mechanism of the films was photochemical or photothermal in nature was beyond the scope of this work yet is an important topic for future research.

This Thesis work offers knowledge on the synthesis and functionalization of gold nanorods. Even though the nanorods were not soluble on liquid-crystal elastomer matrix, this work helps us on the road towards building better photothermal actuators and photomechanical plasmonic substrates in the future.

REFERENCES

[1] H. Yang, J. Liu, Z. Wang, L. Guo, P. Keller, B. Lin, Y. Sun, X. Zhang, Near-infrared-responsive gold nanorod/liquid crystalline elastomer composites prepared by sequential thiol-click chemistry, Chemical Communications, Vol. 51, No. 60, 2015, pp. 12126-12129.

[2] F. Brömmel, D. Kramer, H. Finkelmann, Preparation of Liquid Crystalline Elastomers, in: W. de Jeu (ed.), Liquid Crystals Elastomers: Materials and Applications, 1 ed., Springer, Germany, 2012, pp. 2-48.

[3] H. Jiang, C. Li, X. Huang, Actuators Based on Liquid Crystalline Elastomer Materials, Nanoscale, Vol. 5, No. 12, 2013, pp. 5225-5240.

[4] Z. Mahimwalla, K.G. Yager, J. Mamiya, A. Shishido, A. Priimagi, C.J. Barrett, Azobenzene photomechanics: prospects and potential applications, Polymer Bulletin, Vol. 69, No. 8, 2012, pp. 967-1006.

[5] X. Huang, S. Neretina, M.A. El-Sayed, Gold Nanorods: From Synthesis and Properties to Biological and Biomedical Applications, Advanced Materials, Vol. 21, No. 48, 2009, pp. 4880-4910.

[6] J. Li, H. Guo, Z. Li, Microscopic and macroscopic manipulation of gold nanorod and its hybrid nanostructures Invited, Photonics Research, Vol. 1, No. 1, 2013, pp. 28-41.

[7] T.K. Sau, C.J. Murphy, Seeded High Yield Synthesis of Short Au Nanorods in Aqueous Solution, Langmuir, Vol. 20, No. 15, 2004, pp. 6414-6420.

[8] B. Nikoobakht, M. El-Sayed, Preparation and Growth Mechanism of Gold Nanorods (NRs) Using Seed-Mediated Growth Method, Chemistry of Materials, Vol. 15, No. 10, 2003, pp. 1957-1962.

[9] C.J. Murphy, L.B. Thompson, D.J. Chernak, J.A. Yang, S.T. Sivapalan, S.P. Boulos, J. Huang, A.M. Alkilany, P.N. Sisco, Gold nanorod crystal growth: From seed-mediated synthesis to nanoscale sculpting, Current Opinion in Colloid & Interface Science, Vol. 16, No. 2, 2011, pp. 128-134.

[10] L. Vigderman, B.P. Khanal, E.R. Zubarev, Functional gold nanorods: synthesis, self-assembly, and sensing applications, Advanced materials, Vol. 24, No. 36, 2012, pp. 4811.

[11] X. Huang, M.A. El-Sayed, Gold nanoparticles: Optical properties and implementations in cancer diagnosis and photothermal therapy, Journal of Advanced Research, Vol. 1, No. 1, 2010, pp. 13-28.

[12] J. Pérez-Juste, I. Pastoriza-Santos, L.M. Liz-Marzán, P. Mulvaney, Gold nanorods: Synthesis, characterization and applications, Coordination Chemistry Reviews, Vol. 249, No. 17–18, 2005, pp. 1870-1901.

[13] C.J. Orendorff, C.J. Murphy, Quantitation of Metal Content in the Silver-Assisted Growth of Gold Nanorods, The Journal of Physical Chemistry B, Vol. 110, No. 9, 2006, pp. 3990-3994.

[14] J. Yang, J. Wu, Y. Wu, J. Wang, C. Chen, Organic solvent dependence of plasma resonance of gold nanorods: A simple relationship, Chemical Physics Letters, Vol. 416, No. 4–6, 2005, pp. 215-219.

[15] L. Scarabelli, A. Sanchez-Iglesias, J. Perez-Juste, L.M. Liz-Marzan, A 'Tips and Tricks' Practical Guide to the Synthesis of Gold Nanorods, The Journal of Physical Chemistry Letters, Vol. 6, No. 21, 2015, pp. 4270-4279.

[16] L. Xu, H. Kuang, L. Wang, C. Xu, Gold nanorod ensembles as artificial molecules for applications in sensors, Journal of Materials Chemistry, Vol. 21, No. 42, 2011, pp. 16759-16782.

[17] X. Ye, L. Jin, H. Caglayan, J. Chen, G. Xing, C. Zheng, V. Doan-Nguyen, Y. Kang, N. Engheta, C.R. Kagan, C.B. Murray, Improved Size-Tunable Synthesis of Monodisperse Gold Nanorods through the Use of Aromatic Additives, ACS Nano, Vol. 6, No. 3, 2012, pp. 2804-2817.

[18] C.J. Murphy, T.K. Sau, A.M. Gole, C.J. Orendorff, J. Gao, L. Gou, S.E. Hunyadi, T. Li, Anisotropic Metal Nanoparticles: Synthesis, Assembly, and Optical Applications, The Journal of Physical Chemistry B, Vol. 109, No. 29, 2005, pp. 13857-13870.

[19] Sigma-Aldrich, web page. Available (accessed 10.10.2016): https://www.sigmaaldrich.com/.

[20] L. Scarabelli, M. Grzelczak, L.M. Liz-Marzan, Tuning Gold Nanorod Synthesis through Prereduction with Salicylic Acid, Chemistry of Materials, Vol. 25, No. 21, 2013, pp. 4232-4238.

[21] A. Serrano-Montes, D.J. de Aberasturi, J. Langer, J. Giner-Casares, L. Scarabelli, A. Herrero, L.M. Liz-Marzan, A General Method for Solvent Exchange of Plasmonic Nanoparticles and Self-Assembly into SERS-Active Monolayers, Langmuir, Vol. 31, No. 33, 2015, pp. 9205-9213.

[22] A.W. Hauser, D. Liu, K.C. Bryson, R.C. Hayward, D.J. Broer, Reconfiguring Nanocomposite Liquid Crystal Polymer Films with Visible Light, Macromolecules, Vol. 49, No. 5, 2016, pp. 1575-1581.

[23] A.S.D.S. Indrasekara, R.C. Wadams, L. Fabris, Ligand Exchange on Gold Nanorods: Going Back to the Future, Particle & Particle Systems Characterization, Vol. 31, No. 8, 2014, pp. 819-838.

[24] H. Takahashi, T. Niidome, T. Kawano, S. Yamada, Y. Niidome, Surface modification of gold nanorods using layer-by-layer technique for cellular uptake, Journal of Nanoparticle Research, Vol. 10, No. 1, 2008, pp. 221-228.

[25] S. Kittler, S. Hickey, T. Wolff, A. Eychmuller, Easy and Fast Phase Transfer of CTAB Stabilised Gold Nanoparticles from Water to Organic Phase, Zeitschrift für Physikalische Chemie, Vol. 229, No. 1-2, 2014, pp. 235-245.

[26] M.G. Soliman, B. Pelaz, W.J. Parak, P. del Pino, Phase Transfer and Polymer Coating Methods toward Improving the Stability of Metallic Nanoparticles for Biological Applications, Chemistry of Materials, Vol. 27, No. 3, 2015, pp. 990-997.

[27] L. Blinov, Structure and Properties of Liquid Crystals, 1st ed. Springer Netherlands, London, 2011, 439 p.

[28] C. Ohm, M. Brehmer, R. Zentel, Applications of Liquid Crystalline Elastomers, in: W. de Jeu (ed.), Liquid Crystals Elastomers: Materials and Applications, 1 ed., Springer, Germany, 2012, pp. 95-118.

[29] C. Tschierske, Fluorinated Liquid Crystals: Design of Soft Nanostructures and Increased Complexity of Self-Assembly by Perfluorinated Segments, in: C. Tschierske (ed.), Liquid Crystals Materials Design and Self-assembly, 1 ed., Springer-Verlag Berlin Heidelberg, London, 2012, pp. 1-108.

[30] C. Ohm, M. Brehmer, R. Zentel, Liquid Crystalline Elastomers as Actuators and Sensors, Advanced Materials, Vol. 22, No. 31, 2010, pp. 3366-3387.

[31] M. Sims, L. Abbott, S. Cowling, J. Goodby, J. Moore, Dyes in Liquid Crystals: Experimental and Computational Studies of a Gues-Host-System Based on a Combined DFT and MD Approach, Chemistry (Weinheim an der Bergstrasse, Germany), Vol. 21, No. 28, 2014, pp. 10123-10130.

[32] A. Sengupta, Topological Microfluidics: Nematic Liquid Crystals and Nematic Colloids in Microfluidic Environment, 1st ed. Springer International Publishing, 2016, 153 p.

[33] X. Liu, R. Wei, P.T. Hoang, X. Wang, T. Liu, P. Keller, Reversible and Rapid Laser Actuation of Liquid Crystalline Elastomer Micropillars with Inclusion of Gold Nanoparticles, Advanced Functional Materials, Vol. 25, No. 20, 2015, pp. 3022-3032.

[34] T. White, D. Broer, Programmable and adaptive mechanics with liquid crystal polymer networks and elastomers, Nat Mater, Vol. 14, No. 11, 2015, pp. 1087-1098.

[35] Young's modulus, Encyclopedia of Britannica, web page. Available (accessed 5.11.2016): https://global.britannica.com/science/Youngs-modulus.

[36] H. Finkelmann, E. Nishikawa, G.G. Pereira, M. Warner, A New Opto-Mechanical Effect in Solids, Physical Review Letters, Vol. 87, No. 1, 2001, pp. 015501.

[37] J.E. Marshall, E.M. Terentjev, Photo-sensitivity of dye-doped liquid crystal elastomers, Soft Matter, Vol. 9, No. 35, 2013, pp. 8547-8551.

[38] N. Torras, K.E. Zinoviev, C.J. Camargo, E.M. Campo, H. Campanella, J. Esteve, J.E. Marshall, E.M. Terentjev, M. Omastová, I. Krupa, P. Teplický, B. Mamojka, P. Bruns, B. Roeder, M. Vallribera, R. Malet, S. Zuffanelli, V. Soler, J. Roig, N. Walker, D. Wenn, F. Vossen, F.M.H. Crompvoets, Tactile device based on opto-mechanical actuation of liquid crystal elastomers, Sensors and Actuators A: Physical, Vol. 208, 2014, pp. 104-112.

[39] H. Yoon, S. Kang, M. Lehmann, J.O. Park, M. Srinivasarao, S. Kumar, Homogeneous and homeotropic alignment of bent-core uniaxial and biaxial nematic liquid crystals, Soft Matter, Vol. 7, No. 19, 2011, pp. 8770-8775.

[40] A. Priimagi, Polymer-Azobenzene Complexes: From Supramolecular Concepts to Efficient Photoresponsive Polymers, dissertation, TKK Dissertations 183, 2009, 52 p. Available: http://lib.tkk.fi/Diss/2009/isbn9789522481016/.

[41] K. Yager, C. Barret, Azobenzene Polymers for Photonic Applications, in: Y. Zhao, T. Ikeda (ed.), Smart Light-Responsive Materials, 1 ed., A John Wiley & Sons, INC., Publication, New Jersey, 2009, pp. 1-46.

[42] A. Shimamura, A. Priimagi, J. Mamiya, T. Ikeda, Y. Yu, C.J. Barrett, A. Shishido, Simultaneous Analysis of Optical and Mechanical Properties of Cross-Linked Azobenzene-Containing Liquid-Crystalline Polymer Films, ACS Applied Materials & Interfaces, Vol. 3, No. 11, 2011, pp. 4190-4196.

[43] X. Ye, M.G. Kuzyk, Photomechanical response of disperse red 1 azobenzene dye-doped PMMA polymer fiber, Optics Communications, Vol. 312, 2014, pp. 210-215.

[44] N. Dawson, M. Kuzyk, J. Neal, P. Luchette, P. Palffy-Muhoray, Cascading of liquid crystal elastomer photomechanical optical devices, Optics Communications, Vol. 284, No. 4, 2011, pp. 991-993.

[45] Y. Ji, J.E. Marshall, E.M. Terentjev, Nanoparticle-Liquid Crystalline Elastomer Composites, Polymers, Vol. 4, No. 1, 2012, pp. 316-340.

[46] L. Guo, M. Liu, S.M. Sayed, B. Lin, P. Keller, X. Zhang, Y. Sun, H. Yang, A calamitic mesogenic near-infrared absorbing croconaine dye/liquid crystalline elastomer composite, Chemical Science, Vol. 7, No. 7, 2016, pp. 4400-4406.

[47] D. Smith, B. Korgel, The Importance of the CTAB Surfactant on the Colloidal Seed-Mediated Synthesis of Gold Nanorods, Langmuir, Vol. 24, No. 3, 2008, pp. 644-649.

[48] C. Todaro, Centrifugation, in: H. Vogel, C. Todaro (ed.), Fermentation and Biochemical Engineering Handbook, 3 ed., William Andrew Publishing, Boston, 2014, pp. 267-281.

[49] M. Mozafari, A. Ramedani, Y.N. Zhang, D.K. Mills, Thin films for tissue engineering applications, in: J. Griesser (ed.), Thin Film Coatings for Biomaterials and Biomedical Applications, 1 ed., Woodhead Publishing, 2016, pp. 167-195.

[50] R.F. Egerton, Physical Principles of Electron Microscopy, 1st ed. Springer US, United States of America, 2005, 202 p.

[51] R. Anderson, D. Bendell, P. Groundwater, Organic Spectroscopic Analysis: Ultraviolet-Visible (UV-Vis) Spectroscopy, in: E.W. Abel (ed.), Organic Spectroscopic Analysis, 1 ed., Royal Society of Chemistry, 2004, pp. 7-23.

[52] D. Murphy, M. Davidson, Fundamentals of Light Microscopy and Electronic Imaging, 2nd ed. Wiley-Blackwell, New Jersey, 2012, 554 p.

[53] R.J. Ross, Microelectronics Failure Analysis Desk Reference, 6th ed. ASM International, 2011, 674 p.

[54] T. Kim, C. Lee, S. Joo, K. Lee, Kinetics of gold nanoparticle aggregation: Experiments and modeling, Journal of colloid and interface science, Vol. 318, No. 2, 2008, pp. 238-243.

[55] W.M. Haynes, CRC handbook of chemistry and physics, 97th ed. CRC Press, Boca Raton, Florida, USA, 2016, 2652 p.

APPENDIX 1: TEM IMAGE OF AQUEOUS GNR SOLUTIONS WITH 5-BROMOSALISYLIC ACID

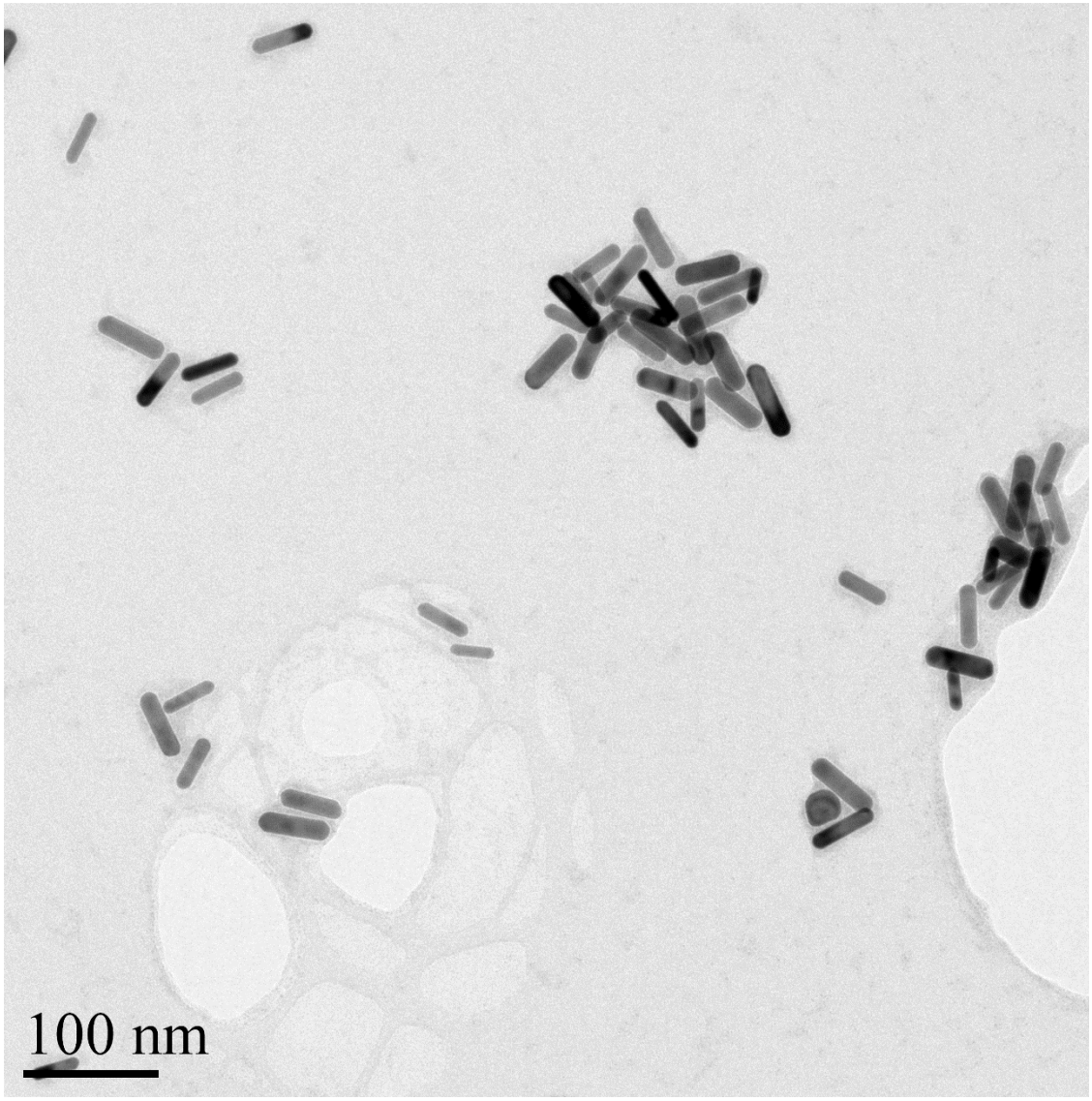

APPENDIX 2: TEM IMAGE OF AQUEOUS GNR SOLUTIONS WITHOUT 5-BROMOSALISYLIC ACID